Investigating Ground-Level Ozone Pollution in Semi-Arid and Arid Regions of Arizona Using WRF-Chem v4.4 Modeling

Yafang Guo[1], Chayan Roychoudhury[1], Mohammad Amin Mirrezaei[1], Rajesh Kumar[2], Armin Sorooshian[1,3], Avelino F. Arellano[1,3]

[1] *Department of Hydrology and Atmospheric Sciences*, *The University of Arizona, Tucson, AZ, USA*

[2] *Research Applications Laboratory, National Center for Atmospheric Research, Boulder, CO, USA*

[3] *Department of Chemical and Environmental Engineering*, *The University of Arizona, Tucson, AZ, USA*

Corresponding to: Yafang Guo (guoy1@arizona.edu)

Abstract. Ground-level ozone (O_3) pollution is a persistent environmental concern, even in regions that have made efforts to reduce emissions. This study focuses on the state of Arizona, which has experienced elevated O_3 concentrations over past decades containing two non-attainment areas designated by the U.S. Environmental Protection Agency. Using the Weather Research and Forecasting with Chemistry (WRF-Chem) model, we examine O_3 levels in the semi-arid and arid regions of Arizona. Our analysis focuses on the month of June between 2017 and 2021, a period characterized by high O_3 levels before the onset of the North American Monsoon (NAM). Our evaluation of the WRF-Chem model against surface Air Quality System (AQS) observations reveals that the model adeptly captures the diurnal variation of hourly O_3 levels and the episodes of O_3 exceedance through the maximum daily 8-hour average (MDA8) O_3 concentrations. However, the model tends to overestimate surface NO_2 concentrations, particularly during nighttime hours. Among the three cities studied, Phoenix (PHX) and Tucson (TUS) exhibit a negative bias in both hourly and MDA8 O_3 levels, while Yuma demonstrates a relatively larger positive bias. The simulated mean hourly and MDA8 O_3 concentrations in Phoenix are 44.6 and 64.7 parts per billion (ppb), respectively, compared to observed values of 47.5 and 65.7 ppb, resulting in mean negative biases of -2.9 ppb and -1.0 ppb, respectively.

Furthermore, the analysis of the simulated ratio of formaldehyde (HCHO) to NO_2 ($HCHO/NO_2$; FNR), reveals interesting insights of the sensitivity of O_3 to its precursors. In Phoenix, the FNR varies from a VOC (volatile organic compound)-limited regime in the most populated areas to a transition between VOC-limited and NO_x-limited regimes throughout the metro area with an average FNR of 1.15. In conclusion, this study sheds light on the persistent challenge of ground-level O_3 pollution in semi-arid and arid regions, using the state of Arizona as a case study.

1. Introduction

Ground-level ozone (O_3), or tropospheric O_3, is a harmful air pollutant that affects human health and plants (Anderson, 2009; Reich, 1987; Iriti and Faoro, 2009; Wang et al., 2017; Lippmann, 1989; Manisalidis et al., 2020). O_3 concentrations are affected by meteorological conditions as well as the concentrations of precursors (Vingarzan, 2004; Wang et al., 2017; Fiore et al., 2002; Jacob, 2000; Monks et al., 2015). Meteorological factors include intensity of solar radiation, temperature (T), relative humidity (RH), winds, pressure, and boundary layer height (Trainer et al., 2000). The precursors of O_3 include nitrogen oxides (NO_x) and volatile organic compounds (VOCs). Besides its significant role in forming O_3, NO_x, particularly NO_2, is also an important pollutant mainly emitted by human activities.

With projections indicating the expansion of aridity zones due to climate change in the future (Asadi Zarch et al., 2017; Achakulwisut et al., 2019; Straffelini and Tarolli, 2023; Huang et al., 2017), there is an anticipated rise in O_3 levels under more drought and elevated temperature conditions (Achakulwisut et al., 2019), thereby posing potential challenges to overall air quality, vegetation, and public health. In the face with these projections, there is an undeniable sense of urgency in advancing our comprehension of O_3 production mechanisms and refining forecasting model skills, especially within urban arid regions. This imperative arises from the acknowledgement that urban areas in arid climates face a distinctive set of challenges marked by exceptionally low precipitation, elevated temperatures, and unique vegetation. Gaining such insights is crucial for generating effective strategies to mitigate the negative impacts on air quality, vegetation, and the health of urban populations in response to shifting climatic conditions.

Because of the Clean Air Act, average NO_2 concentrations have decreased substantially in the U.S. since the 1990s (U.S. Environmental Protection Agency [EPA], National Emissions Inventory

(NEI) air pollutant emissions trends data, http://www.epa.gov/ttnchie1/trends/, 2012, hereinafter referred to as EPA, online report, 2012). For example, the annual 98th percentile of daily maximum 1-hour average NO_2 was reduced from 42 ppb to 33 ppb with a 21% decrease in the national average from 2010 to 2022 (Epa, 2023). VOCs in the atmosphere are generally emitted from two major sources: human activity and biogenic volatile organic compounds (BVOCs) produced by plants. In the U.S., VOC emissions data are tracked by the NEI. According to NEI data, in Maricopa County, where the city of Phoenix resides, total estimated VOC emissions from anthropogenic sources, excluding forest wildfires and prescribed burns, decreased by 35% between 2008 and 2020 (from 0.19 million tons to 0.13 million tons). Most anthropogenic emissions reductions were observed among on-road mobile sources and other industrial processes. As a result, O_3 levels have substantially decreased across much of the U.S. (Cooper et al., 2012; Parrish et al., 2022). In 2015, the U.S. EPA lowered the O_3 National Ambient Air Quality Standard (NAAQS) to 70 parts per billion (ppb). The design value is defined as the annual fourth-highest maximum daily 8-h average (MDA8) O_3 concentration, averaged over three years. Any area that does not meet this standard is designated as a nonattainment area (NAA). Despite the nationwide decrease of O_3 precursors and O_3 concentrations, there are still areas where O_3 levels exceeded the 2015 NAAQS standard of 70 ppb in 2017 (U.S. EPA Green Book 8-h Ozone 2015). Therefore, for these areas, it is critical to have a detailed understanding of the chemical and meteorological processes influencing O_3 formation so that better pollution control can be put in place to reduce O_3 levels.

Identifying and quantifying the various sources that contribute to the formation of O_3 is challenging due to the complicated nature of atmospheric chemistry and variability of O_3 precursors (Duan et al., 2008; Fang et al., 2021; He et al., 2019; Odman et al., 2009; Yang et al., 2021; Zare et al., 2014; Zhan et al., 2023; Trainer et al., 2000). First, O_3 formation is a complex process that involves the interaction of multiple precursor pollutants, such as NO_x and VOCs, under the influence of sunlight. The chemistry behind these reactions can be highly nonlinear and dependent on numerous variables (e.g., temperature, moisture, cloud cover, and solar radiation) (Trainer et al., 2000). This nonlinearity makes it challenging to predict how changes in emissions will impact O_3 concentrations. In addition, O_3 is not limited to areas where its precursors are emitted as it can be transported over long distances. This makes it difficult to attribute O_3 levels

solely to local sources, as regional and even global factors can influence local concentrations (Vingarzan, 2004; Monks et al., 2015).

In Arizona, the Phoenix-Mesa metropolitan area is currently designated as a moderate NAA for O_3 and has ranked among the top five of most polluted cities for O_3 in the recent 5 years (source: https://www.lung.org/research/sota/city-rankings/most-polluted-cities). Another NAA is Yuma County. Unlike Maricopa County, Yuma is a rural region that has a much lower population and emissions. With Yuma being located on the border of Mexico on the south/southwest and California on the west, its O_3 levels thus are significantly impacted by both international and inter-state transport. Qu et al. (2021) investigated the sources of O_3 pollution in Yuma, Arizona, and found strong international influences from Northern Mexico on 12 out of 16 O_3 exceedance days. They also performed a sensitivity study with the GEOS-Chem model and found that reducing emissions in Arizona alone would have a minimal impact on mitigating O_3 exceedances in Yuma, with only a 0.7% reduction in MDA8 O_3. In contrast, reducing emissions in Mexico is estimated to contribute to an 11% reduction in O_3 during these exceedances, bringing MDA8 O_3 in Yuma below the standard. Li et al. (2015) applied WRF-Chem with sensitivity experiments and showed that Arizona emissions have a dominant impact on MDA8 O_3 concentrations in Phoenix, while southern California's contributions range from a few ppb to over 30 ppb.

While long-range transport of precursors and O_3 into Arizona does occur, the primary contributor to O_3 levels remains the in-situ production resulting from local emissions. Because most of Arizona is a semi-arid and arid region with a unique southwest natural environment including weather, climate, and desert plants, it is important to understand how the extreme heat, low moisture, and year-around desert shrubs contribute to O_3 production in order to minimize O_3 exceedances and improve air quality forecasting (Sorooshian et al., 2024). Additionally, even though Arizona is a typical desert weather region with high temperatures and low moisture year-round, during the North American Monsoon (NAM) the primary wind flow in Arizona shifts from westerly/southwesterly to southerly/southeasterly, resulting in elevated moisture from the Pacific Ocean and the Gulf of California. Furthermore, unlike the other O_3 polluted regions in the Eastern US, which are mainly forest ecosystems, most of Arizona experiences little precipitation—less than 25 centimeters or 25 to 50 centimeters of rain per year (Paul et al., 2002). The BVOCs are also quite unique in the arid climate region. Geron et al. (2006) found out that in the Mojave and

Sonoran Desert regions of the western US where Arizona is, of all the 13 common desert plant species, only two of the species emitted isoprene (most abundant BVOC) indicating that this type of ecosystem is not likely a strong source of isoprene, compared to forest ecosystems.

In section 2 we first discuss the climatology of Phoenix, as a representation of southwest Arizona, and then describe the datasets employed and the setup of the WRF-Chem model. In section 3 we present analyses of model evaluation with observations including meteorological fields, O_3, and precursors. The analyses of O_3 exceedance and VOC-NO_x sensitivity are also included. Section 4 summarizes the main conclusions of this study.

2. Data and Method

This research focuses on the study of O_3 in the state of Arizona in the U.S. In this section, we begin with introducing the available datasets applied to evaluate the WRF-Chem model including observational datasets from EPA AQS and PAMS network, reanalysis using CMAQ modeling, radiosonde measurements, and regional forecasts. Then a description of the study region is given following by the model description and configurations.

2.1 EPA AQS surface observations

We use the hourly and daily surface in situ observations of O_3, CO, NO_2, and meteorological fields such as T, RH, and winds from the EPA AQS monitoring network (Demerjian, 2000). Sites within each city were selected based on their availability during the study periods for each parameter. For instance, for O_3 measurements, 10 sites were selected in Phoenix, 7 in Tucson, and 2 in Yuma. The information for each is listed in Table S2. For evaluation purposes, we applied quality control to the raw data to exclude any values that were zero or negative before doing further analysis. To calculate the MDA8 O_3, any days with more than 8 continuous hourly data points missing were excluded from the analysis. Zero and negative values were treated as missing while values below the method detection limit (MDL) were replaced with 0.5×MDL (Zhang et al., 2012).

2.2 EPA PAMS VOC measurements

The network of Photochemical Assessment Monitoring Stations (PAMS) established by the U.S. EPA plays a crucial role in monitoring and understanding ground-level O_3 pollution in affected areas providing measurements of various O_3 precursors, including VOCs. The list of measurements includes 63 different compounds with some of the most common VOC species like

formaldehyde (HCHO), acetaldehyde, acetone, ethanol, and two monoterpenes (α-pinene and β-pinene; $C_{10}H_{16}$). The primary objective of these PAMS sites is to create a comprehensive database of O_3 precursors and meteorological conditions to better understand local O_3 formation, support the development of O_3 models, and allow for the tracking of important trends in O_3 precursor
150   concentrations over time. The two PAMS monitor sites in Arizona are located in Phoenix (JLG Supersite: 04-013-9997) and Tucson (22nd & Craycroft: 04-019-1011). The sampling frequency for most VOCs is hourly averaged. For formaldehyde, JLG supersite uses the EPA's 3-day schedule with three 8-hour averaged carbonyl samples per day on every third day.

2.3 Radiosonde data

155   High vertical resolution temperature profiles from radiosondes are applied to determine the planetary layer boundary height (PBLH) for WRF-Chem evaluations. Data from radiosondes launched at three different locations (Phoenix, Tucson, and Yuma) were downloaded. The radiosonde launches in Phoenix are active during the monsoon season, starting in mid-June and ending in late September while Tucson and Yuma conduct regular daily balloon launches. The
160   launch times for Phoenix and Tucson are set at 0000 UT and 1200 UT, while Yuma operates two launch sites with schedules at 1200 UT, 1800 UT, and 2100 UT. To estimate the PBLH, we use the Bulk Richardson Number Method. Richardson number is a dimensionless number used to assess atmospheric stability. The top of planetary layer boundary is marked by when the Richardson number exceeds a threshold of 0.25.

165   **2.4 CMAQ reanalysis**

A high-resolution (12 x 12 km^2) air quality reanalysis over the contiguous U.S. (CONUS) is available from 2005-2018 (https://www.gcseglobal.org/development-air-quality-products). This reanalysis is generated using a newly developed chemical data assimilation system that simultaneously assimilates aerosol optical depth (AOD) retrievals from the Moderate Resolution
170   Imaging Spectroradiometer (MODIS) and carbon monoxide (CO) retrievals from the Measurement of Pollution in the Troposphere (MOPITT) in the Community Multiscale Air Quality (CMAQ) model. The WRF model provides meteorological input for CMAQ simulations over the CONUS. This dataset offers a suite of air quality products, e.g. $PM_{2.5}$, PM_{10}, O_3, NO_2. In this study, beyond the ground-based EPA observations we expand our analysis by incorporating this
175   reanalysis dataset to enhance the evaluation of O_3 levels across Arizona.

2.5 ADEQ forecasts

The Arizona Department of Environmental Quality (ADEQ) produces five-day hourly air quality forecasts for locations across Arizona (https://www.azdeq.gov/forecast). Specifically for our study region, forecasts are released Monday through Friday and include O_3, PM_{10}, and $PM_{2.5}$. The forecast values are for the monitor with the highest MDA8 O_3 concentration for a given day within the Phoenix-Mesa NAA and the Tucson area, whereas for Yuma it is a single monitor (Yuma Supersite).

2.6 Description of study region and time period

The climate of the south and southwest parts of Arizona (Sonoran Desert) is dry and hot, with much of the region characterized as arid. Our primary interest is in three major cities: Phoenix, Tucson, and Yuma. Phoenix, the most populated city, is designated as an O_3 NAA by EPA along with the entire metro area; Tucson, which is the second largest city in the state, experiences mild O_3 pollution but gets stronger influence from the monsoon and Mexico; Yuma, situated near both California and Mexico, is a representation of an arid section of the Sonoran Desert and also designated as a NAA with clean data determination by EPA.

Shown in Figure 1 are the monthly mean surface air values of MDA8 O_3, CO, NO_2, and meteorological fields of RH, T, wind speed, and wind direction in the city of Phoenix. These monthly values were derived from averaging the daily EPA AQS data collected over a 5-year period from 2017 to 2022 at the Phoenix JLG Supersite. The MDA8 (Figure 1a) exhibits peaks during the summer months, spanning from April to September, except for the year 2020 when the COVID-19 pandemic began. On the other hand, the monthly CO, NO_2, and RH show an opposite trend, with their lowest values observed during the summer months. RH is the lowest in June and then increases as the monsoon arrives in July, followed by decreases in September after the monsoon ends. Besides the COVID-19 factor, 2020 is ranked as the second driest year in Arizona's history, with a statewide precipitation level of only 6.63 inches (Nws Phoenix, 2020). Figure 1(d) shows that the RH levels during late 2020 (red line) and early 2021 (purple line) were the lowest across the five-year period. Additionally, the temperature during the summer of 2020 (Figure 1e) was also the highest. For winds, the windiest seasons are spring and summer, and the wind direction varies throughout the year. The wind direction is determined by taking the inverse tangent of the total zonal and meridional wind components, which are derived from the daily maximum

wind speed and its corresponding direction. Summer months exhibit mostly westerly winds and winter months consist of more easterly winds (Figure 1f-1g). Shown in Figure 1h is the distribution of monthly O_3 exceedance days at the JLG supersite in Phoenix (site number: 04-013-9997). An O_3 exceedance day occurs when the MDA8 O_3 is greater than 70 ppb on that day. The exceedance days are mostly recorded from April to September, referred to here as the "ozone season". In the months of June and July in the year 2020, the MDA8 O_3 (Figure 1a) and exceedance days (Figure 1h) were substantially lower than in other years and the reason could be related to the COVID-19 pandemic. The pandemic's stay-at-home period resulted in much lower traffic levels and hence reduced anthropogenic emissions.
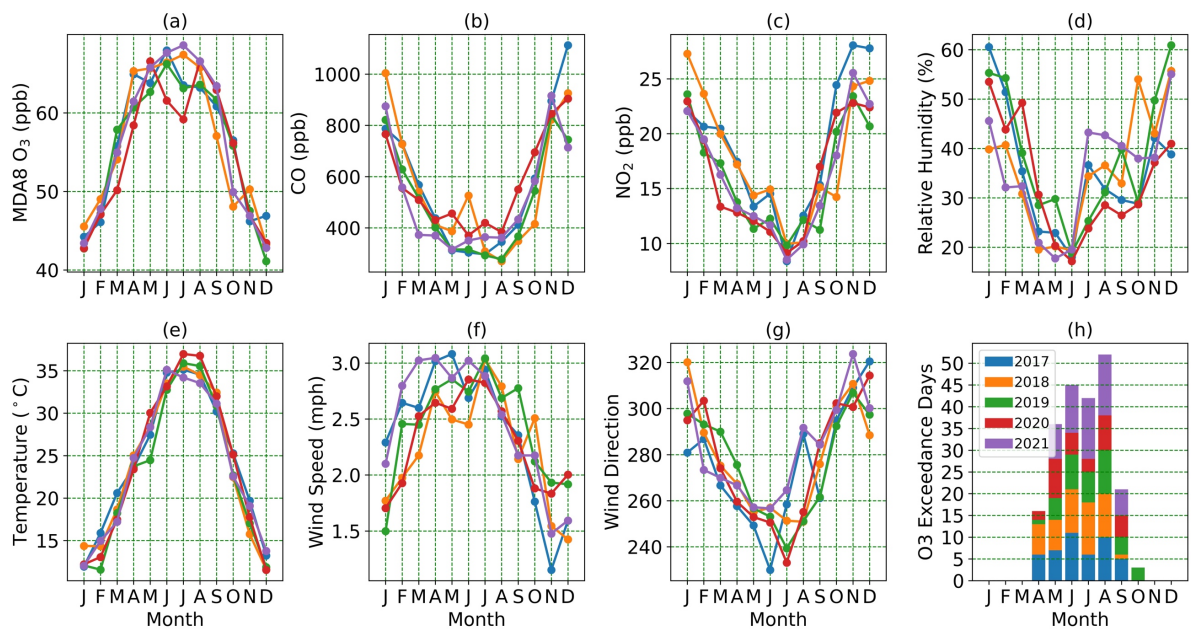
Figure 1. Monthly mean of Phoenix surface (a) MDA8 O_3, (b) CO, (c) NO_2, (d) relative humidity (RH), (e) temperature (T), (f) wind speed, (g) wind direction, and (h) number of exceedance days for years between 2017 and 2021, derived from EPA criteria gases and meteorological daily summary data of a single site (Phoenix JLG supersite).

Based on these monthly results, we choose the month of June (dry summer), when O_3 levels, temperature, and winds are high, and the moisture level is still low. It is also intended to mitigate the impact of the heavy precipitation that typically accompanies the monsoon. Additionally, since we focus on the desert area, dust storm events can significantly impact the O_3 photolysis, hence the concentrations. According to Lader (2016), the highest frequency of dust storm events happens

during the active Monsoon season (in July and August). Therefore, we have chosen June as our main study period to reduce the impacts of dust. We apply the WRF-Chem model (v4.4) with state-of-art configurations to simulate the O_3 concentrations over Arizona. Numerical simulations were conducted during June between 2017 and 2021 for a total of five years. Furthermore, the ozone season in 2017 was also simulated as our base year. The following sections describe the datasets analyzed herein and the configuration used for the WRF-Chem simulations.

2.7 WRF-Chem setup

The Weather Research Forecasting coupled with Chemistry (WRF-Chem) (Grell et al., 2005) model is a fully coupled meteorology-chemistry transport model developed by the National Center for Atmospheric Research (NCAR). This study uses WRF-Chem v4.4 to simulate O_3 in Arizona. With our ultimate goal of establishing an operational forecasting and analysis system for Arizona in the future, we have configured the model using the NCAR WRF-Chem forecasting system as a reference (https://www.acom.ucar.edu/firex-aq/forecast.shtml). The comprehensive parametrization schemes are provided in the following list. The Model for Ozone and Related Chemical Tracers (MOZART-4, (Emmons et al., 2010)) is selected for the gas-phase chemistry, coupled with the Goddard Chemistry Aerosol Radiation and Transport (GOCART, (Chin et al., 2002)) for aerosol chemistry with wet scavenging enabled. The standard MOZART-4 mechanism includes 85 gas-phase species, 12 bulk aerosol compounds, in addition to 39 photolysis and 157 gas-phase reactions. It also includes an updated isoprene oxidation scheme and a better treatment of volatile organic compounds, with three lumped species to represent alkanes and alkenes with four or more carbon atoms and aromatic compounds (called BIGALK, BIGENE and TOLUENE) (Emmons et al., 2010). The new updated TUV photolysis option, based on standalone TUV version 5.3, is employed to calculate the photolysis rates. This new TUV option uses O_3 climatology distributed from the model top (~20km) to 50 km. Initial and lateral boundary conditions are supplied every six hours from both the Global Forecast System (GFS) with a horizontal grid spacing of $1°$ for meteorology and the Community Atmosphere Model with Chemistry (CAM-Chem) (Lamarque et al., 2012; Tilmes et al., 2015) for chemistry. Biogenic emissions are calculated online with the Model of Emissions of Gases and Aerosols from Nature (MEGAN, v2.1) using the simulated meteorological conditions while running WRF-Chem (Guenther, 2007; Guenther et al., 2006). Note that MEGAN v2.1 currently is only compatible with the CLM4 (Community Land Model Version 4, Oleson et al. 2010) land surface model. The anthropogenic

emissions used in this study are obtained from 2017 National Emissions Inventories (NEI2017) data provided by the US EPA (https://www.epa.gov/air-emissions-inventories/2017-national-emissions-inventory-nei-data) with a 4 km grid resolution covering the US and surrounding land

255   areas. NEI emissions are then interpolated and regridded to model domain grids. Biomass burning emissions are calculated using the Fire Inventory from NCAR (FINNv2.5) (Wiedinmyer et al., 2023) and the online plume-rise model (Freitas et al., 2007). FINNv2.5 is based on fire counts derived from both satellite MODIS and VIIRS (Visible Infrared Imaging Radiometer Suite) active fire detection (Wiedinmyer et al., 2023). We employed the GOCART dust option in accordance

260   with the GOCART aerosol scheme. The following key physics settings are also employed: Morrison double–moment microphysics (Morrison et al., 2009), RRTMG for long and short-wave radiation (Iacono et al., 2008), Eta Similarity for surface layer physics (Monin and Obukhov, 1954), the Unified Noah Land Surface Model (Tewari et al., 2004), the Yonsei University (YSU) planetary boundary layer (PBL) scheme (Hong, 2010), and the Grell–Freitas cumulus

265   parameterization scheme (Grell and Freitas, 2014).

The model is configured with two nested grid domains consisting of 9 km and 3 km horizontal grid spacing along with 34 vertical levels. Shown in Figure 3 is the WRF-Chem domain setup. The parent domain (D01) covers the entire western U.S. with expansion to northern Mexico to better understand the wind shift from Mexico during NAM, while the nested domain (D02, Fig. 2b)

270   focuses on Arizona. Both domains are centered in the Phoenix metropolitan area. D01 features 271 and 394 horizontal grids, while D02 is characterized by 349 and 313 horizontal grids. The topography in Figure 2b (color contours) shows that Phoenix is located in about the center of a valley, called Salt River Valley. The WRF-Chem run periods are specifically designed to be the month of June between 2017 and 2021, with each run consisting of a total of 33 simulation days,

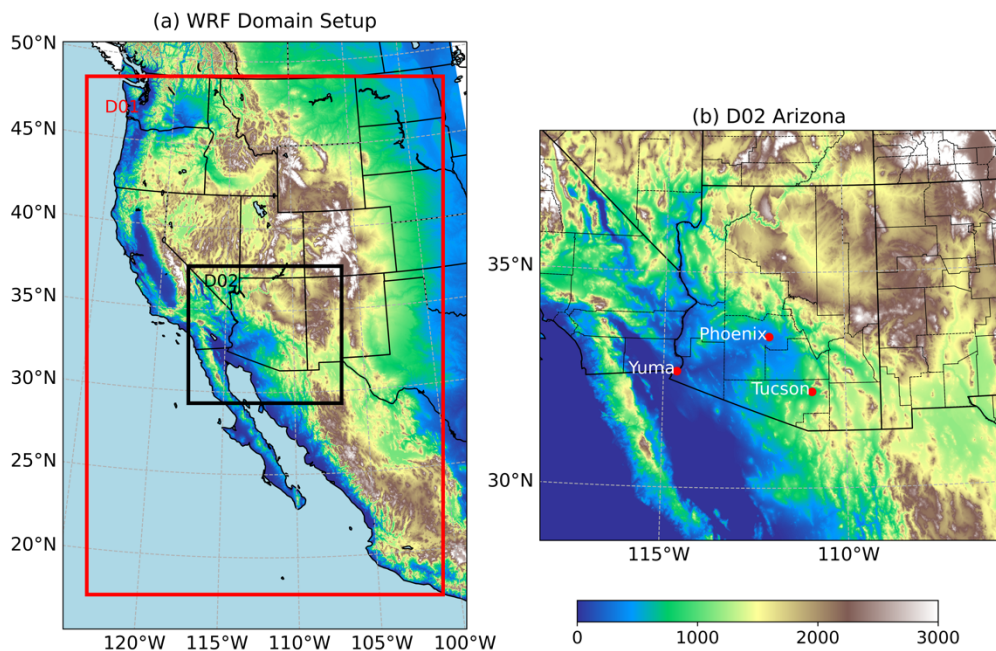275   including a three-day spin-up in late May and 30 days in June.

Figure 2. (a) WRF-Chem domain setup for outer domain D01 and inner domain D02, (b) geographic location of three Arizona cities: Phoenix, Tucson, and Yuma. Black dash lines in (b) represent the county borders. Contours denote the elevation in meters over the continent.

3. Results and Discussion

3.1 Model evaluations

We begin by evaluating the simulated diurnal and monthly variations of meteorological fields and major air pollutants using the AQS monitor site and PAMS observations. Shown in Figure 3 is the time series of Phoenix hourly surface O_3 concentrations in June for the year 2017 and 2018. CMAQ air quality reanalysis datasets are also included for evaluation. The AQS observations for a particular city are calculated as the average of hourly or maximum daily 8-hour average (MDA8) O_3 levels obtained from all selected sites. These observations are subsequently compared with the mean simulated O_3 concentration within the corresponding area. The diurnal pattern of O_3 concentrations is clearly discernible, with peak levels occurring during the afternoon and reaching their lowest points at night. In general, the WRF-Chem model effectively captures these daily O_3 concentration patterns. Conversely, the reanalysis dataset notably underestimates O_3 levels during the nighttime. Notably, in June 2017, an extreme O_3 event occurred, characterized by O_3 levels exceeding 80 ppb and lasting for 9 days, starting on 14 June 2017. On 20 June, O_3 levels even

11

reached 100 ppb. The model effectively simulates this exceptional event, while the reanalysis dataset tends to overestimate this peak.

Listed in Table 1 are the statistical metrics comparing hourly concentrations from the WRF-Chem to the AQS monitoring sites at three different locations: Phoenix (PHX), Tucson (TUS), and Yuma
295   (YUMA). The statistics include Pearson correlation coefficient (R); mean bias (MB); mean error (ME); root mean square error (RMSE); normalized mean bias (NMB); normalized mean error (NME); mean normalized bias (MNB); mean normalized error (MNE); fractional bias (MFB); fractional error (MFE). For hourly O_3, the correlation (R) indicates that all locations show a positive correlation, with PHX having the highest at 0.81, followed by TUS at 0.73, and YUMA
300   at 0.69. The negative MB suggests that in PHX (-2.9 ppb) and TUS (-1.7 ppb) WRF-Chem underestimates the O_3 concentration, while YUMA (5.2 ppb) suggests an overestimate. PHX and TUS generally exhibit smaller biases and errors compared to YUMA. Additionally, YUMA has the highest variability in errors and the highest NME and RMSE values, indicating less agreement with AQS data compared to PHX and TUS.
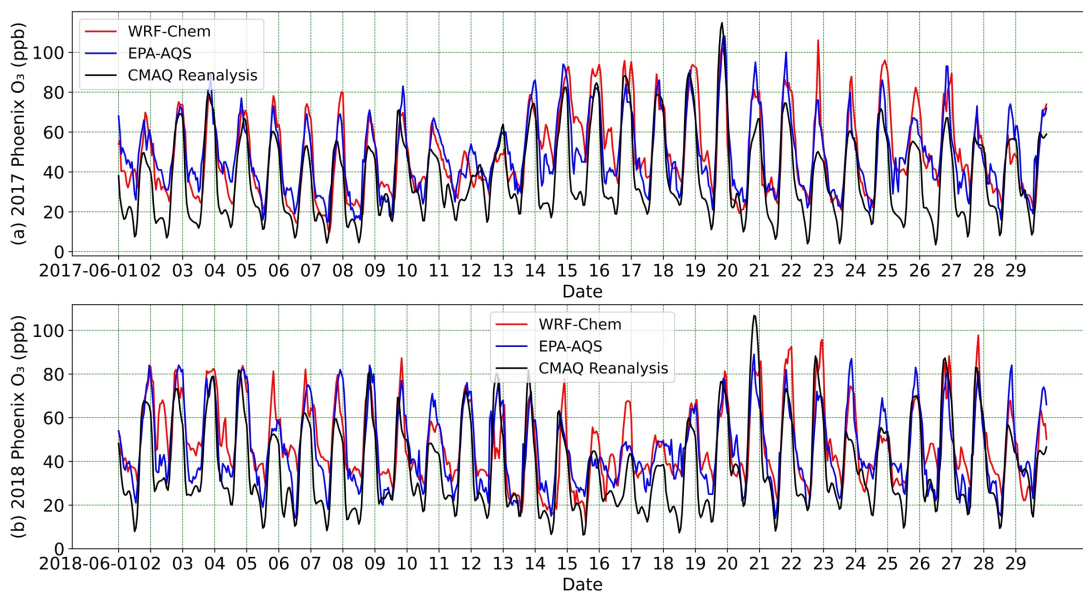

Figure 3. WRF-Chem simulated (red), EPA AQS (blue), and CMAQ reanalysis (black) hourly surface O_3 concentrations in June of 2017 (top) and 2018 (bottom) in Phoenix. Results are at Universal Time.

305

Table 1. Mean statistics of WRF-Chem hourly O$_3$ and evaluation with respect to EPA AQS observations in June for years 2017 to 2021. R: Pearson correlation coefficient; MB: mean bias; ME: mean error; RMSE: root mean square error; NMB: normalized mean bias; NME: normalized mean error; MNB: mean normalized bias; MNE: mean normalized error; MFB: fractional bias; MFE: fractional error.

Hourly O$_3$	WRF, AQS	R	MB	ME	RMSE	NMB (100%)	NME (100%)	MNB	MNE	MFB	MFE
PHX	44.6, 47.5	0.81	-2.9	8.3	10.6	-6.1	17.6	-0.03	0.19	-0.07	0.20
TUS	46.2, 47.9	0.73	-1.7	6.4	8.1	-3.5	13.4	-0.02	0.14	-0.04	-0.37
YUMA	46.3, 41.1	0.69	5.2	9.1	12.6	12.9	22.4	0.26	0.34	0.13	0.61

In addition to the hourly O$_3$ evaluation, we have also examined the MDA8 (Maximum Daily 8-Hour Average) O$_3$. MDA8 O$_3$ is a crucial metric used in air quality management and assessment, as well as a good indicator of air pollution. Shown in Figure 4 are the MDA8 O$_3$ concentrations for June 2017-2021 in the cities of PHX, TUS, and YUMA. Similar to hourly O$_3$ in Figure 3, for the MDA8 O$_3$, we employed the CMAQ reanalysis data and AQS observations for our evaluation. Additionally, since the CMAQ reanalysis data is available only up to the year 2018, we incorporated ADEQ forecasts for the years 2019 through 2021. The statistical results of the MDA8 O$_3$ evaluation against AQS observations can be found in Table 2. Statistics of CMAQ reanalysis and ADEQ forecasts in each individual year are included in Supplement Table S3.

Overall, WRF-Chem MDA8 O$_3$ exhibits a smaller mean bias compared to hourly O$_3$, except Yuma, where the mean bias slightly increases from 5.2 ppb to 6.3 ppb. However, it is worth noting that the correlation coefficients show a slight decrease from 0.81 and 0.73 to 0.66 and 0.62 for PHX and TUS, respectively, compared to hourly O$_3$. This reduction in correlation could be attributed to fewer data points available for linear fitting in the case of MDA8 O$_3$. Additionally, the RMSE at PHX is reduced from 10.6 ppb for hourly O$_3$ to 8.6 ppb for MDA8 O$_3$. Considering statistics in both Tables 1 and 2, we conclude that WRF-Chem exhibits better performance in capturing the variations of MDA8 O$_3$ concentrations than hourly O$_3$.

Furthermore, when we compare WRF-Chem with CMAQ reanalysis, our findings indicate that WRF-Chem demonstrates smaller biases and higher correlations. For instance, the reanalysis

consistently underestimates the MDA8 O_3 at PHX but overestimates them at Yuma during the 4-9 June and 20-28 June periods, as illustrated in Figure 4.
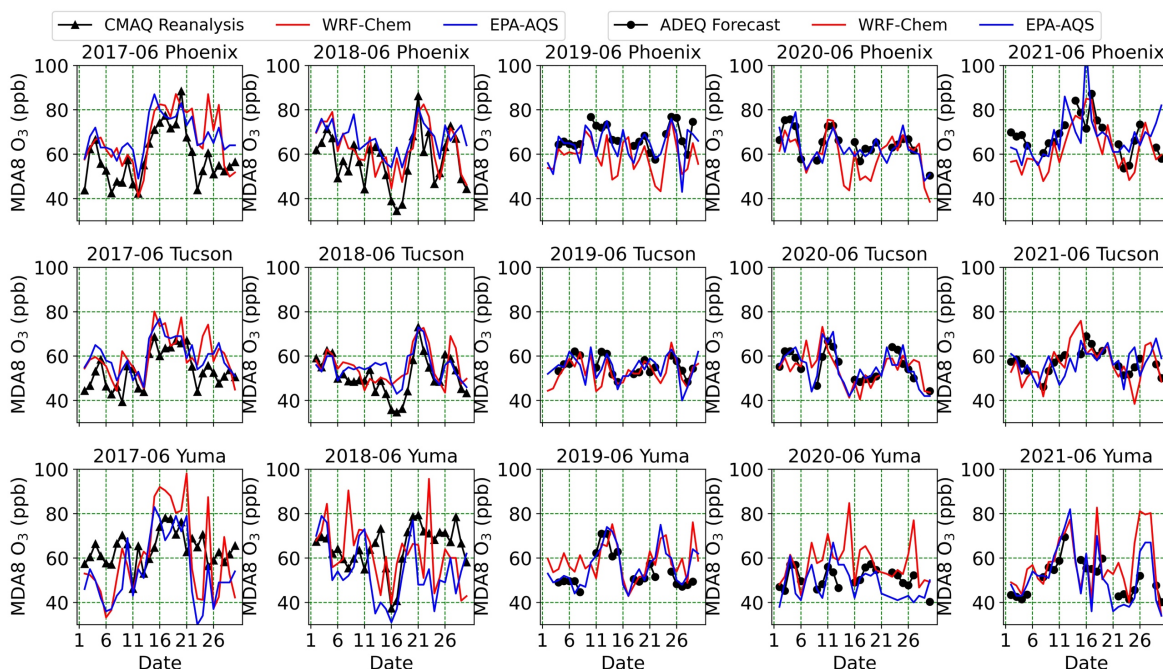

Figure 4. WRF-Chem simulated (red), EPA AQS (blue), and CMAQ reanalysis (black triangle), ADEQ forecasts (black circles) MDA8 O_3 concentrations in June 2017-2021 for three major Arizona cities: Phoenix, Tucson, and Yuma.

Table 2. Same as Table 1, but for MDA8 ozone evaluation.

MDA8 O_3	WRF, AQS	R	MB	ME	RMSE	NMB (100%)	NME (100%)	MNB	MNE	MFB	MFE
PHX	64.7, 65.7	0.66	-1.0	6.9	8.6	-5.6	10.5	-0.05	0.11	-0.06	0.11
TUS	55.9, 56.3	0.62	-0.4	5.1	6.3	-0.8	9.1	-0.00	0.09	-0.01	0.09
YUMA	59.9, 52.9	0.7	6.3	8.7	11.3	12.2	16.5	0.14	0.18	0.11	0.15

Besides O_3 evaluations, we examined other air pollutants and essential meteorological parameters. We present in Figure 5 the daily surface concentrations of CO, NO_2, isoprene, and formaldehyde (HCHO), along with surface T and RH for June 2021. CO and NO_2 are two prominent anthropogenic pollutants and serve as O_3 precursors. Isoprene (the simplest 5-carbon isoprenoid, C5H8) and monoterpene is the dominant BVOC emitted to the atmosphere and accounts for over

14

335 50% of the total BVOC emissions (Guenther et al., 2012). Their concentrations are significantly influenced by factors such as temperature, vegetation, and light conditions (Morrison et al., 2016; Kalogridis et al., 2014). It is important to note that observations of VOCs using the PAMS system, in comparison to the well-established AQS monitoring system, remain relatively limited. Currently, the PAMS monitoring network in Arizona only operates during summer months from

340 June to August and only started in recent years. For instance, of the two PAMS sites within Arizona, only two daily measurements of formaldehyde were recorded in June 2019 in Phoenix, and the observation schedule changed from 1 in 6 days to 1 in 3 days since 2018. In Tucson, formaldehyde observations only became available starting in 2021 with a 1 in 3 days schedule. Daily measurements of isoprene became available in both Phoenix and Tucson starting in 2021.

345 In comparison with the observations, the model appropriately replicated the daily variations of surface T and RH with minimal biases. However, for CO, WRF-Chem failed to capture the elevated episode over PHX during 11-15 June 2021. It is worth noting that during this period there was an active wildfire (Telegraph Fire, situated southeast of Phoenix, https://wfca.com/wildfire-articles/arizona-fire-season/) that lasted one month and became one of the largest wildfires in the

350 U.S. throughout the 2021 wildfire season. Because of this, the CO levels in both Phoenix and Tucson were significantly impacted by the fire plumes with smoke moving right over Phoenix. The model may not be able to simulate the smoke plumes well. Despite the limited PAMS data, we were able to compare the daily isoprene concentrations with observations in both cities. On average, daily mean isoprene is around 5 ppb in PHX and 1 ppb in TUS. Furthermore, for HCHO

355 concentrations, the model is comparable to the observations, not only in terms of the values, but also in capturing their variations. In conclusion, the online biogenic emission model employed in the WRF-Chem model, MEGAN 2.1, effectively simulates the BVOC levels.
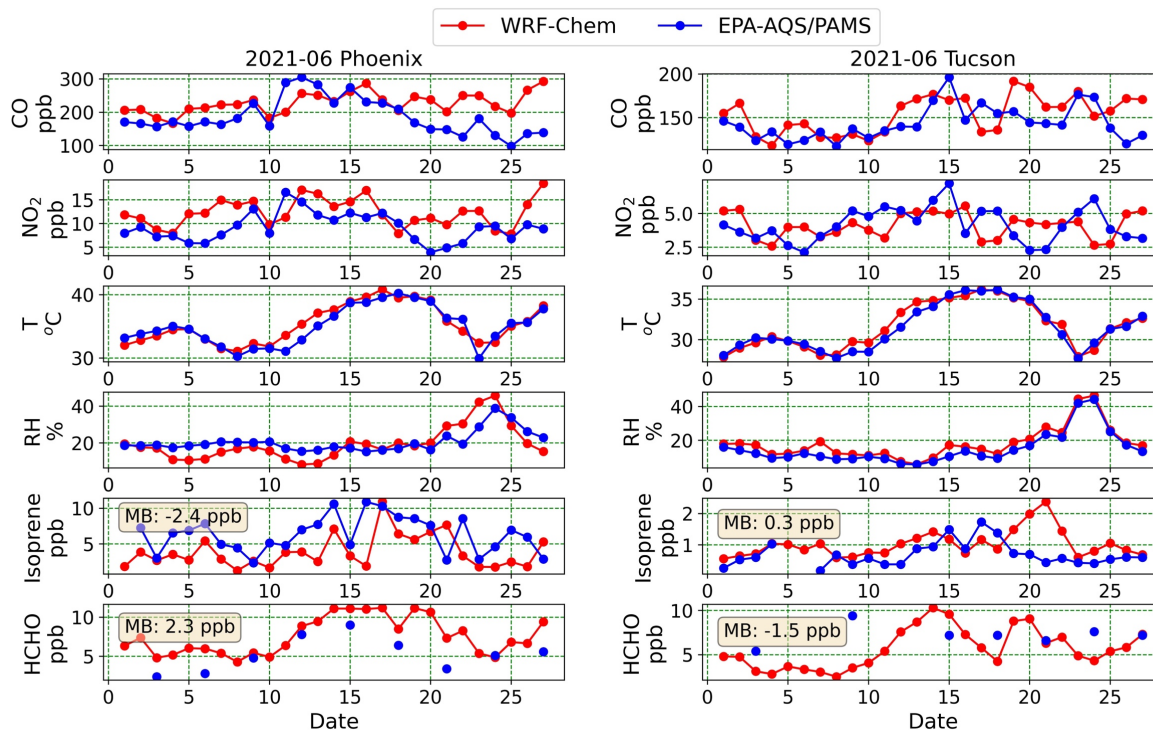
Figure 5. WRF-Chem simulated (red) and EPA observed (blue) surface concentrations of CO and NO₂, surface temperature (T), 2-meter relative humidity (RH), surface concentrations of isoprene and formaldehyde (HCHO) for June 2021. CO, NO₂, T, and RH measurements are obtained through the EPA AQS network. Isoprene and HCHO measurements are acquired from the EPA PAMS networks in PHX and TUS. The mean bias (MB) for isoprene and HCHO are also included.

Figure 6a-6c presents the spatial plots of monthly mean surface concentrations of MDA8 O_3, CO, and NO_2 for June. The contour plots are based on hourly model output between year 2017 and 2021. The colored circles represent the AQS surface observations for three cities: Phoenix (PHX), Tucson (TUS), and Yuma (YUMA). Both the WRF-Chem model and the observations indicate that MDA8 O_3 in the Phoenix metro area reaches up to 65 ppb (Figure 6a). The northeast of PHX, which is a downwind region, experiences significant O_3 pollution as the prevailing winds in June are predominantly southwest winds (Figure 6f). The background O_3 level in most of Arizona is around 50 ppb, while west/southwest Arizona, including Yuma, is substantially influenced by O_3 from California.

For CO concentrations, the highest simulated surface levels in PHX reach 224.2 ppb, closely matching the corresponding AQS measurement of 221.9 ppb (Figure 6b). Downwind of Phoenix, CO concentrations range between 100 to 120 ppb. Hotspots in the southeast direction of both PHX

16

and TUS are associated with wildfire burning events, such as the 2017 Frye Fire (southeast hotspot of TUS) and the 2021 Telegraph Fire. The observed mean NO_2 level in PHX is approximately 5 ppb and is mostly distributed in populated areas as the main source of NO_2 is anthropogenic emissions. An additional figure in the supplement (Figure S1) provides monthly mean O_3, CO, and NO_2 concentrations for individual years.

The aridity of southwest Arizona is characterized by high temperatures and low RH. Shown in Figures 6d-6f are the mean surface temperature, 2-meter RH, and surface winds. Notably, the temperature in PHX is slightly higher than that in TUS as PHX is located in the valley and TUS has a higher elevation (see Figure 2b). The RH overall is under 20% in southwest Arizona, where the Sonoran Desert is located. The climate of the west/southwest and other parts of Arizona is distinctive. The monthly mean wind predominantly comes from the southwest direction, with an average speed of 10 miles per hour (mph).
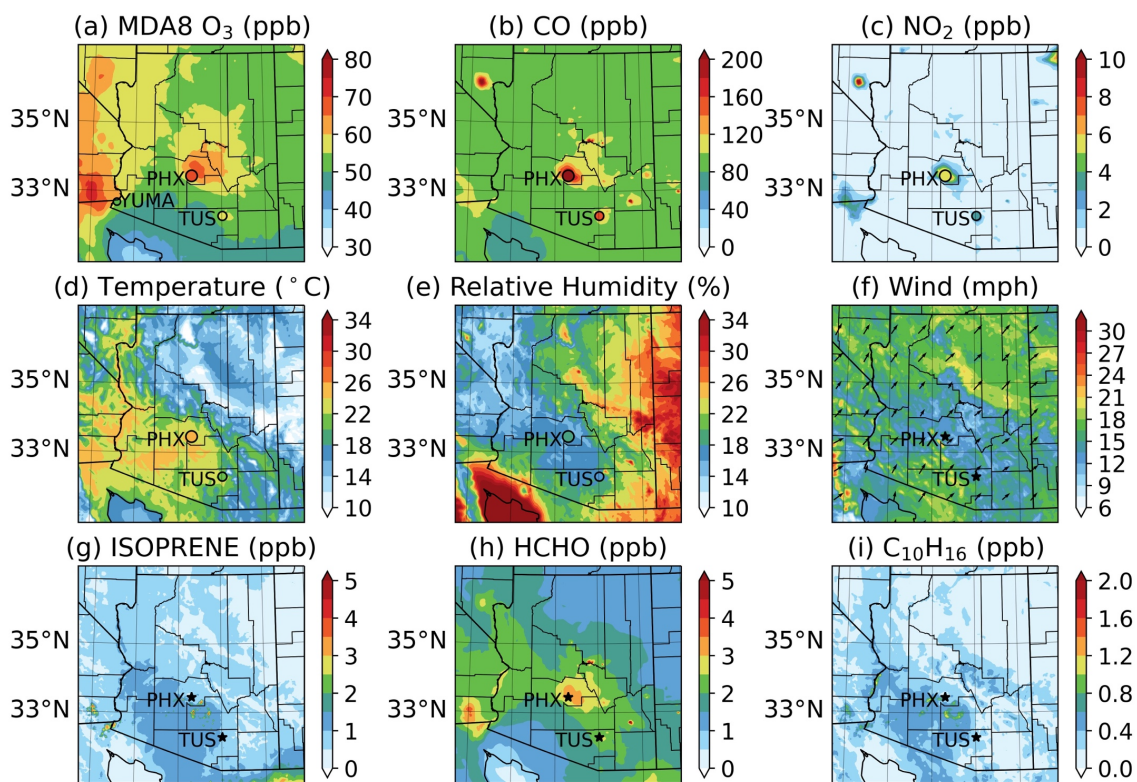
Figure 6. WRF-Chem simulated monthly mean concentrations of main pollutions (O_3, CO, NO_2), meteorological fields (temperature, relative humidity, wind), and major VOCs (isoprene, formaldehyde, and monoterpene). Colored circles represent the EPA AQS site observations for comparison.

Table 3 presents the statistics of CO, NO_2, T, and RH between simulations and observations for PHX and TUS. In general, the simulated values of O_3, CO, and T (temperature) align well with the observations. Temperature shows a small, normalized bias of 2% and -1.3% for PHX and TUS, respectively. The model overestimates CO both in PHX and Tucson by 7.1% and 5.75%, respectively. Additionally, the model overestimates the NO_2 levels in both PHX and TUS. Figure 6g-6i also demonstrates three dominant VOC concentrations: isoprene, formaldehyde (HCHO), and monoterpene ($C_{10}H_{16}$). Overall, the BVOCs are rather small over the desert region, except Yuma, where it is largely impacted by agricultural vegetation.

Table 3. Statistics of WRF-Chem evaluation with respect to EPA AQS monitors. Results represents the average of June across five years between 2017 and 2021.

City	Method	CO (ppb)	NO$_2$ (ppb)	T (°C)	RH (%)
Phoenix	AQS	221.8	9.0	24.8	18.4
	WRF	238.0	9.5	25.3	15.6
	Bias (%)	16.2 (7.1%)	0.5 (5.3%)	0.5 (2%)	-2.8 (-15.2%)
Tucson	AQS	142.1	3.9	24.0	16.3
	WRF	150.2	4.4	23.7	17.1
	Bias (%)	8.1 (5.7%)	0.5 (12.8%)	-0.3 (-1.3%)	0.8 (4.9%)

To further investigate the bias between simulations and observations, in Figure 7, we present the frequency distributions of hourly O$_3$, the corresponding O$_3$ bias with respect to the AQS observations, and MDA8 O$_3$ for June in the five-year period for Phoenix (top), Tucson (middle), and Yuma (bottom). For O$_3$ levels higher than 50 ppb (background O$_3$ level in Arizona), WRF-Chem demonstrates good performance in estimating the distributions in Phoenix and Yuma but tends to overestimate in Tucson, particularly between 50 to 60 ppb. Furthermore, WRF-Chem fails to capture the extremely high O$_3$ observational days exceeding 70 ppb for all three cities. Conversely, for low O$_3$ levels below 50 ppb, which are more associated with nighttime O$_3$, WRF-Chem substantially underestimates the values. Therefore, for bias analysis, we divide the assessment into daytime and nighttime periods to account for the diurnal variability of O$_3$ formation. The middle panel in Figure 7 presents the fractional bias of hourly O$_3$ between WRF-Chem and AQS observations. In general, during the daytime the mean bias is positive (Figure 7b, 7e, 7h) suggesting an overestimation by WRF-Chem, while a negative mean bias during the night indicates that WRF-Chem underestimates the hourly O$_3$ values in PHX. The MDA8 O$_3$ distribution demonstrates better overall agreement between the model and observations than hourly O$_3$, consistent with the statistics in Tables 1 and 2.
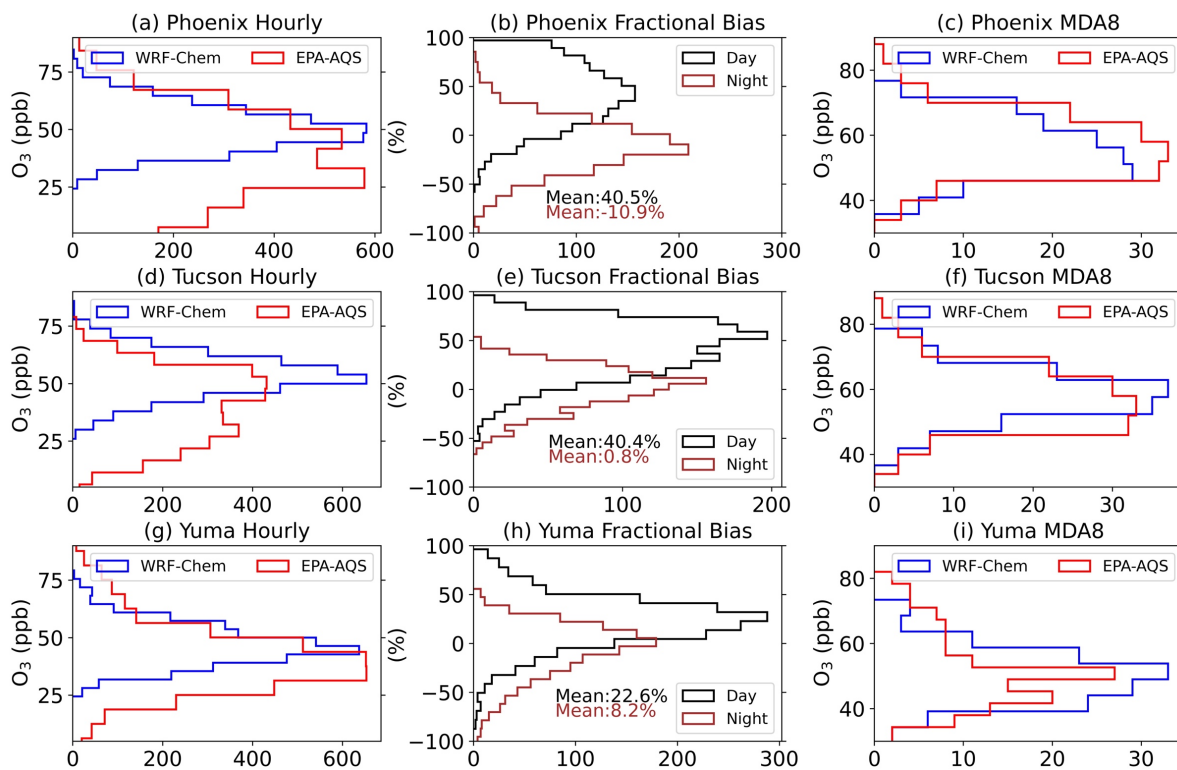
Figure 7. Model evaluation for cities of Phoenix (top row), Tucson (middle row), and Yuma (bottom row). The first panel in each row shows observed (red) and WRF-Chem simulated (blue) surface O₃ frequency distribution; the second panel is the frequency distribution of model bias for both daytime (black) and nighttime(brown); the third panel presents the frequency distribution of MDA8 O₃.

410

To gain deeper insights into the factors contributing to O_3 bias between daytime and nighttime, the distribution of surface NO_2 concentration is presented in Figure 8. For data quality purposes, surface NO_2 concentrations that are less than 0.5 ppb are discarded for both simulations and observations. Similar to O_3, the model misrepresents large NO_2 episodes in PHX and TUS when NO_2 is greater than 40 ppb and 15 ppb, respectively. There is a larger diurnal variability in the observations than in simulations. The simulated NO_2 distribution during daytime and night are comparable while observed distributions are significantly different with distinct slopes (Figure 8a, 8d). In PHX, the model overestimates the high NO_2 levels (>10 ppb) during the night while in TUS, the model underestimates the NO_2 during the daytime. The mean bias for day and night in PHX are 0.2 ppb and 1.9 ppb, respectively. The mean bias for day and night in TUS is -2.4 ppb

20

and 0.5 ppb, respectively. The bias over Tucson suggests that WRF-Chem overestimates the NO_2 during the night.
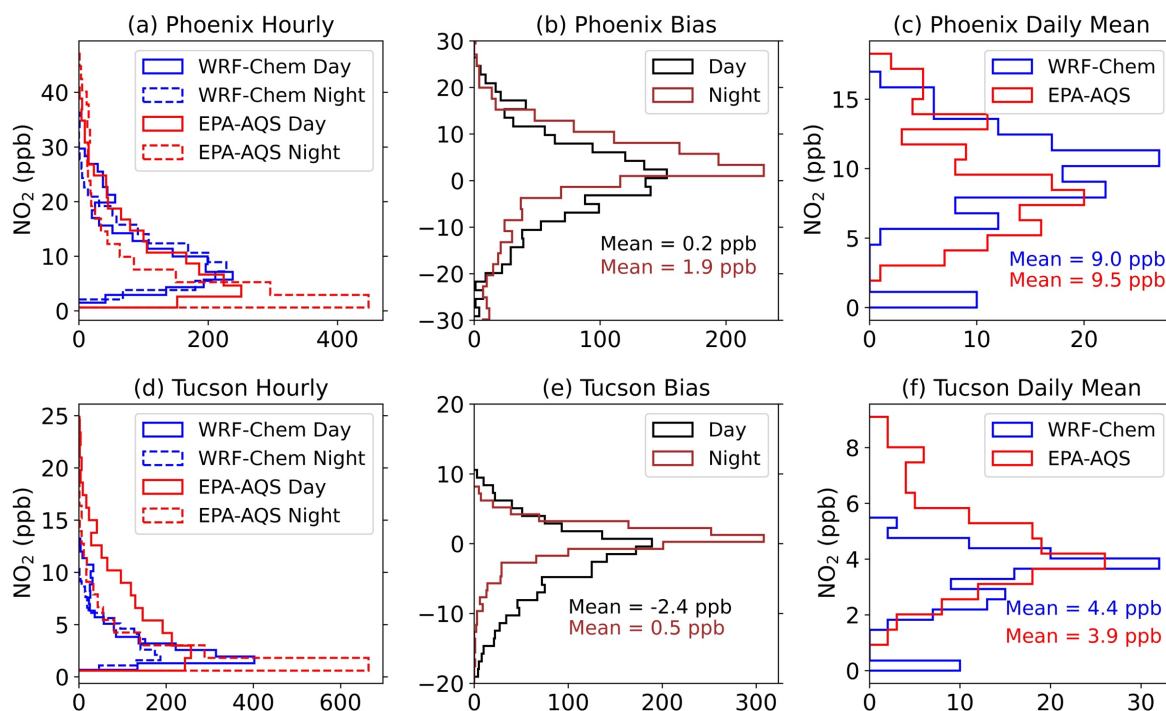

Figure 8. Same as Figure 7, but for surface NO₂ concentrations at two cities: PHX (top) and TUS (bottom). From left to right panels: hourly surface NO₂ distributions, NO₂ fractional bias, daily mean NO₂ distributions. Hourly NO₂ distributions on the left panel are divided into day and night times.

425

To address the biases depicted in Figure 8 during daytime and nighttime, the PBLH is investigated. A higher PBLH allows pollutants and aerosols to disperse and mix with cleaner air over a larger vertical extent, resulting in a reduction of air pollutant concentrations. Consequently, an overestimation of PBLH leads to an underestimation of O_3 and NO_2, and conversely, an underestimation of PBLH may contribute to overestimations of these pollutant levels. Using the radiosonde data, we estimated the PBLH at three cities and compared with model simulations. The launching times of radiosondes at Arizona sites are at Universal Time (UT) hours of 12:00, 21:00, and 00:00, which correspond to Local Time (LT) hours of 05:00, 14:00, and 17:00, respectively.

435 Presented in Figure 9 are the PBLH for three cities, PHX, TUS, and YUMA, during June 2018 (additional years' data are available in the supplement). The nighttime soundings launched at LT 05:00 are highlighted with red stars, and their corresponding WRF-Chem simulated PBLH values are represented as red dots. Conversely, daytime soundings are indicated by blue markers. Simulated PBLH at all other times without sounding data are labeled with grey dots. It is worth

440 noting that the WRF-Chem model consistently demonstrates an underestimate of PBLH during nighttime (as denoted by the red markers) and an overestimate during daytime (as shown by the blue markers). The mean daytime bias of PBLH between model and observations at Phoenix (LT 17:00), Tucson (LT 14:00), and Yuma (LT 14:00) are 322.0 m, 18.1 m, and 602.5 m, respectively. These biases are closely related to the MDA8 O_3 bias listed in Table 2 where bias in Phoenix is

445 larger than Tucson. The nighttime biases are all negative with values of -509.7 m, -435.4 m, -55.8 m, indicating an overall underestimate. The underestimate of PBLH during the night will cause the shallower vertical mixing of daytime accumulated O_3 leading to the positive bias of nighttime O_3 observed in Figure 7.
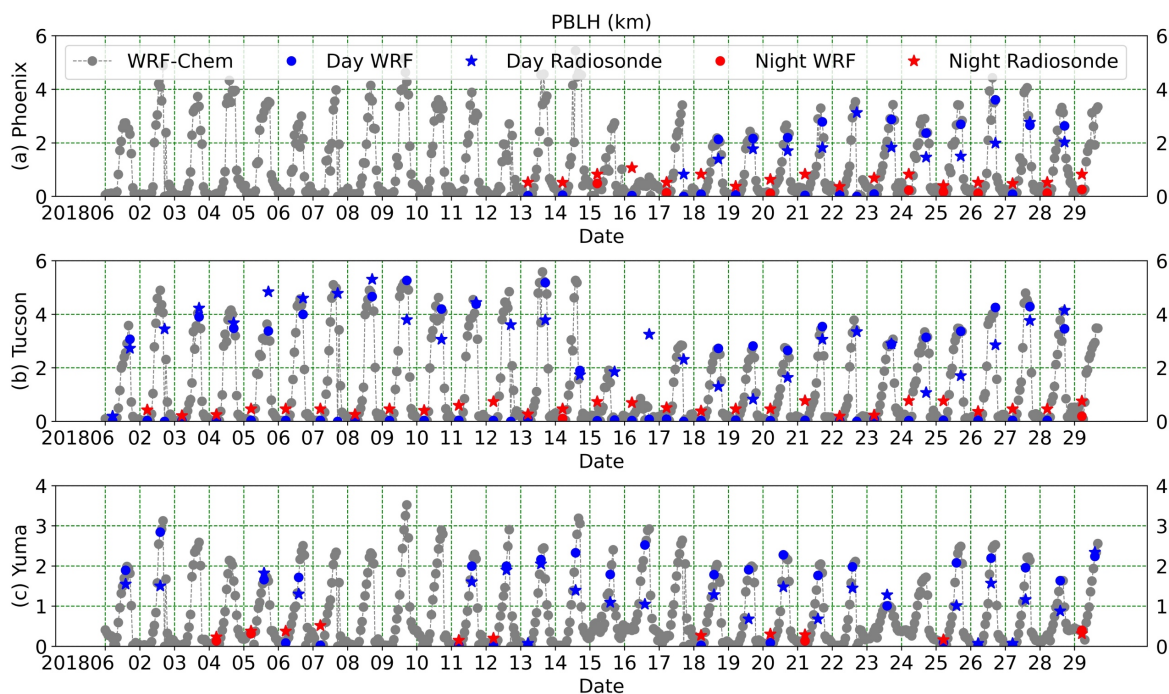
Figure 9. Planetary boundary layer height (PBLH) in June 2018 for three cities: (a) Phoenix, (b) Tucson, and (c) Yuma. Dots and stars represent simulation from WRF-Chem and observation from radiosondes, respectively. Nighttime PBLH estimated from radiosonde data at 05:00 local time are denoted as red stars, with their corresponding simulated PBLH values indicated as red dots. Blue markers represent radiosondes launched during daytime with corresponding WRF-Chem simulations denoted by blue dots.

450

3.2 O₃ Exceedance

According to the EPA, an exceedance day occurs on each calendar day when the MDA8 O_3 concentration is greater than 70 ppb, where 70 ppb is the ground-level O_3 standard from the 2015 National Ambient Air Quality Standards (NAAQS). A design value, on the other hand, is a statistic

455   that describes the air quality status of a given location relative to the NAAQS level. The O_3 design value of the Phoenix-Mesa metropolitan area has increased from 76 ppb in 2017 to 81 ppb in 2022 (refer to Table S1 in the Supplements). The rising and persisting O_3 levels led to the reclassification of Phoenix-Mesa metropolitan area from a marginal to a moderate non-attainment status for O_3 limits by the EPA. In the previous section, we demonstrated that WRF-Chem exhibits good

460   performance in simulating the mean O_3 and other precursor parameters. Moreover, the model performs better with the MDA8 O_3. To further investigate the issue of O_3 pollution in Phoenix,

23

this section focuses on O_3 exceedances. As depicted in Figure 1, O_3 exceedances typically first start in April and last occur in September, with the exception of the year 2019 when exceedances extended into October, and the year 2021 when no exceedance was observed in April. Over the five-year period from 2017 to 2021, in the greater Phoenix area, the average annual count of O_3 exceedance days was 43. Even in 2020, amidst the onset of the COVID-19 pandemic and the enforcement of stay-at-home measures, which resulted in reduced concentrations of NO_x, O_3 exceedances in Phoenix did not exhibit significant reduction. Figure 10(c) illustrates the boundary of the designated Maricopa County non-attainment area (NAA, depicted by polygons outlined in black), along with the locations of AQS sites equipped for O_3 monitoring. In total, there are 29 monitoring sites, with 27 of them situated within the NAA boundary.

Presented in Figure 10 are the spatial variations of the mean O_3, MDA8 O_3, and count of O_3 exceedance days for June 2017 within the Maricopa County NAA. In the top panel (Figures 10a-c), we depict the monthly mean surface hourly O_3 concentrations as derived from WRF-Chem, CMAQ reanalysis, and data from AQS monitor sites. These 27 AQS sites, encompassing a range of urbanization levels, population densities, and downwind/upwind positions, exhibit considerable variability even within the NAA. Figures 10(d-f) show the monthly mean MDA8 O_3 concentrations, with higher levels observed in the northeastern part of the NAA, a pattern accurately captured by both WRF-Chem and the reanalysis. Better agreement among model and observations is evident considering both hourly and MDA8 O_3. The reanalysis data substantially underestimates the mean hourly O_3 levels by 10 ppb but captures the MDA8 O_3 spatial distribution pattern. Lastly, the count of O_3 exceedance days is shown in Figure 10(g-i). The exceedance days vary from 2 to 10 days within the area. The regions with the highest population density, particularly the central Phoenix-Mesa region, exhibit the highest counts of exceedance days. Additionally, since the prevailing wind in June is westerly (Figures 1 and 6), the east side of the valley is observed with higher O_3 levels. In general, the model exhibits strong agreement with the observational data regarding factors such as location, number of days, spatial extent, and spatial variability.
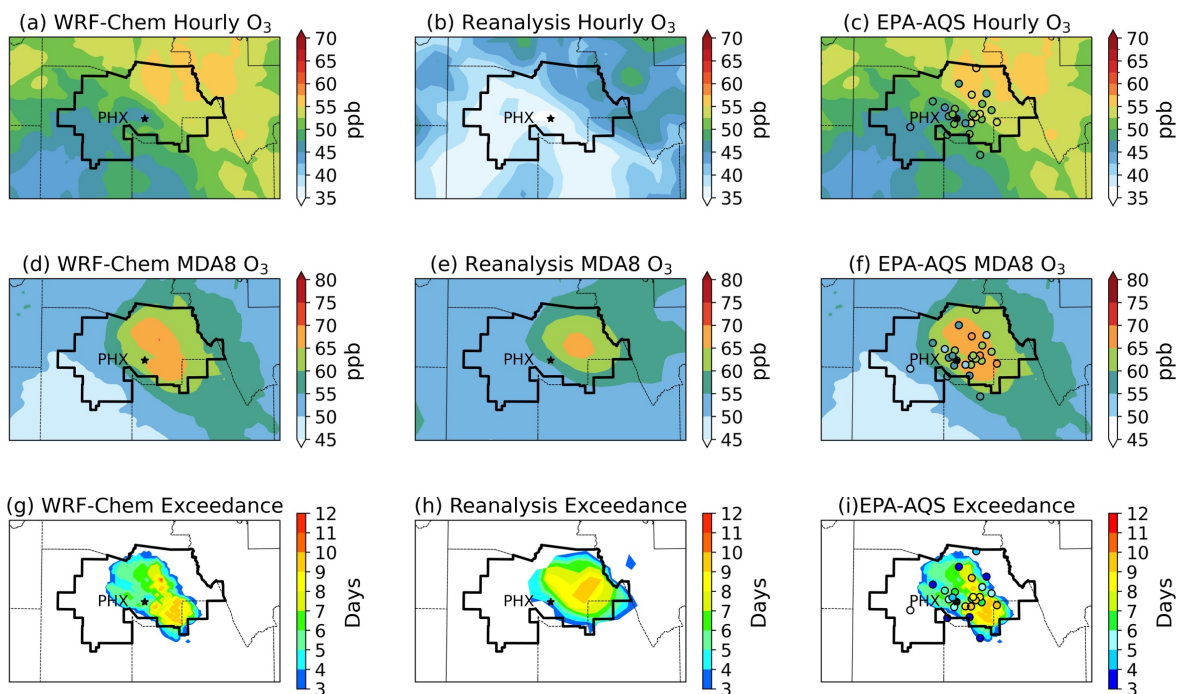
Figure 10. Comparison of WRF-Chem simulation (left column), CMAQ reanalysis (middle column), and EPA AQS observations (colored circles) overlaid with WRF-Chem results (right column) depicting monthly mean surface hourly and MDA8 O_3 concentrations (top and middle), and exceedance days (bottom) in June 2017. O_3 exceedance is defined as a day when the MDA8 concentration exceeds 70 ppb. The Phoenix-Mesa non-attainment area is bounded by black curves.

3.3 O_3 source attribution

Source attribution of O_3 is challenging due to the complex processes that control O_3 formation. Tropospheric O_3 levels are influenced by a multitude of factors including 1) meteorological factors, such as T, RH, cloud cover, radiation, wind speed and direction, precipitation, and boundary layer height; 2) O_3 precursors, such as NO_x, VOCs, and CO, which can originate from biomass burning (wildfire, prescribed fire), biogenic emissions, and anthropogenic emissions; and 3) O_3 transport, such as long-range transport and stratospheric O_3 intrusions. Understanding the relationships between these factors and O_3 levels is essential for discerning their respective impacts on ambient O_3 concentrations. Several analytical methods are available for investigating O_3 source attributions, e.g., backward trajectory analysis (Xiong and Du, 2020; Dimitriou and Kassomenos, 2015; Betito et al., 2023; Betito et al., 2024), machine learning algorithm (Cheng et al., 2023; Mishra et al., 2023; Weng et al., 2022), and chemistry models (Butler et al., 2020; Lupaşcu and Butler, 2019; Sudo and Akimoto, 2007). In this paper, we employ scatter plots that utilize both

model outputs and ground observations. These scatter plots serve as a practical means to delve deeper into the intricate connections between O_3 and its major influencing factors, aiding in the identification and quantification of their contributions to O_3 concentrations in the atmosphere.

Figure 11 presents a series of scatter plots that illustrate the relationships between O_3 concentrations and other key variables, including CO, NO_2, surface T, and RH during daylight hours at the Phoenix JLG Supersite. The data points are color-coded, with green denoting simulations and orange representing observations. Each column panel within the figure corresponds to the respective month of June for individual years spanning from 2017 to 2021. The displacement between the orange and green dots on the first row suggests that WRF-Chem overestimates the CO concentrations in all the years except 2018. In the years 2017 and 2021, more extreme O_3 concentrations were present with levels exceeding 100 ppb.

The negative correlation between NO_2 and O_3 (depicted in Figure 11f-j) reveals that in Phoenix, surface O_3 levels tend to be higher when NO_2 concentrations are lower. When hourly NO_2 levels exceed 25 ppb, O_3 concentrations generally remain below 60 ppb. Furthermore, the positive correlation between temperature and O_3 suggests that in general elevated temperatures are associated with higher O_3 levels. It is worth noting that on some extreme hot days, O_3 levels can also be low. Conversely, the negative correlation between RH and O_3 indicates that increased RH tends to be linked with lower O_3 concentrations. These intricate relationships offer valuable insights into the complex interplay between O_3 and its influencing factors within the Phoenix JLG Supersite region.
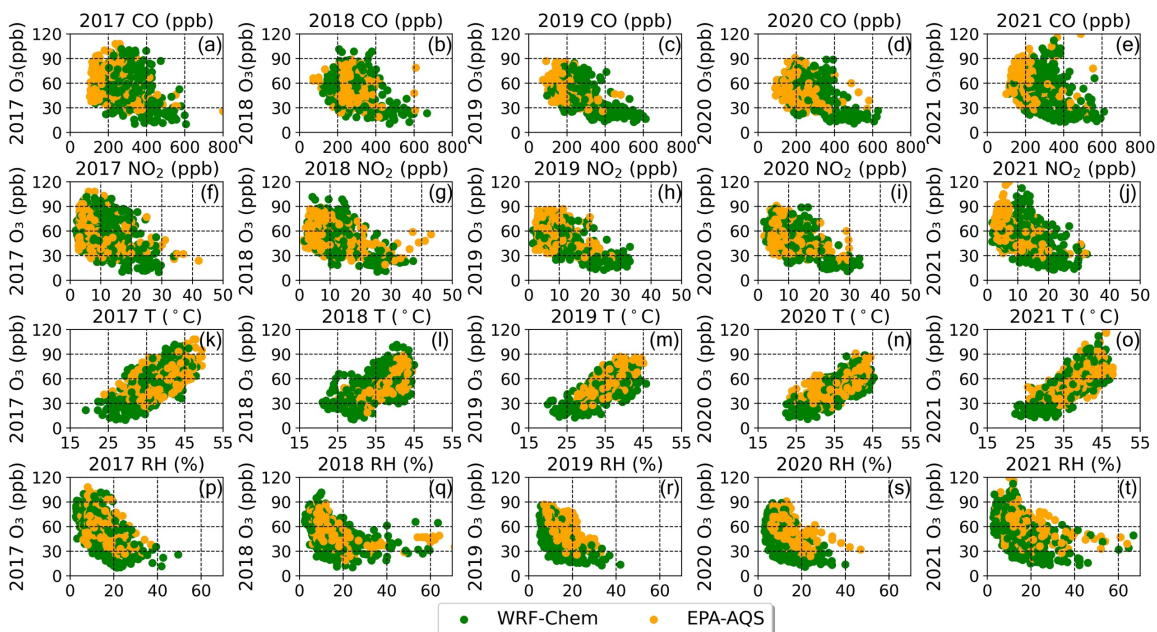
Figure 11. WRF-Chem simulated (green) and EPA AQS (orange) hourly CO, NO₂, surface temperature (T), and relative humidity (RH) versus hourly O₃ concentration during the daytime.

As previously discussed in earlier sections, the O_3 exceedance in Arizona can be originated from a combination of various contributing factors, which can be classified into two main categories: local production and transport. Notably, on 13 June 2017, the observed surface O_3 levels in both Phoenix and Yuma experienced a substantial increase, with a MDA8 concentration of approximately 90 ppb in Phoenix. This particular event has been successfully captured by both the WRF-Chem model and CMAQ reanalysis, as illustrated in Figure 4. Shown in Figure 12 are the simulated vertical profiles of O_3, CO, NO_2, and HCHO, as well as the surface meteorological parameters including PBLH, temperature (T), 500 mb height, and RH during this extreme event. The simulated and AQS observed MDA8 O_3 are also included for reference. During the event, both the surface and columnar concentrations of CO, NO_2, and HCHO were all elevated, particularly in the boundary layer. In the meantime, PBLH and RH decreased, while temperature and 500 mb height increased, consistent with the correlation relationships observed in Figure 11. Furthermore, we employed the Hybrid Single-Particle Lagrangian Integrated Trajectory model (HYSPLIT) (Rolph et al., 2017; Stein et al., 2015) to calculate 48-hour back-trajectories for the 13 June exceedance event, as illustrated in supplementary Figure S5. As depicted in Figure 12, at the onset of the extreme events on June 13, 2017, temperatures were lower compared to previous days.

However, as the event progressed, a heat episode emerged over Phoenix following a decrease in PBLH. The 48-hour back trajectories suggest a potential influence of airmasses (O_3 or its precursors) originating from California or Asia contributing to the elevated O_3 levels observed in Phoenix on June 13, 2017. Subsequently, in the following days, the high O_3 concentrations are more associated with local production.
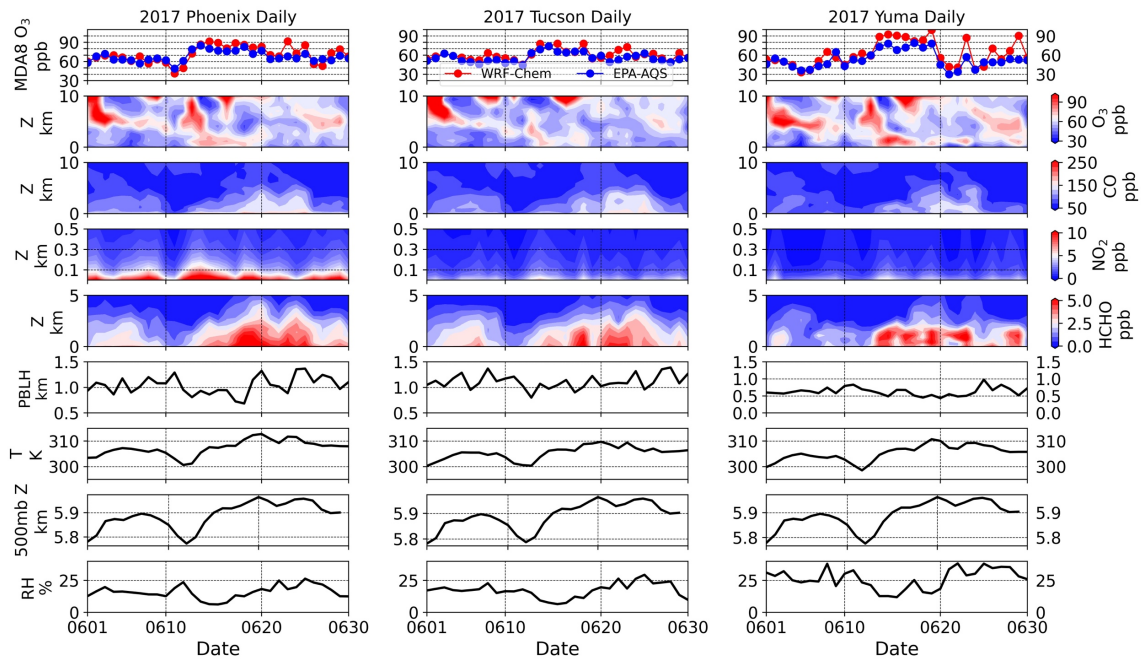

Figure 12. Vertical profiles of simulated O_3, CO, NO_2, and HCHO at three cities (contour plots) along with the surface MDA8 O_3 (top panel), PBLH, surface temperature (T), 500 mb height, and surface relative humidity (RH) in June 2017. An O_3 exceedance event on 13 June was observed in all three cities.

3.4 O_3-NO_X-VOC sensitivity

The O_3-NO_x-VOC sensitivity is a crucial concept in the fields of atmospheric chemistry and air quality management (Duncan et al., 2010; Sillman, 1995; Sillman and He, 2002; Sillman et al., 2003; Liu and Shi, 2021; Carrillo-Torres et al., 2017; Zaveri et al., 2003). It refers to how the concentration of O_3 in the atmosphere responds to changes in the levels of NO_x and VOCs. Understanding this sensitivity is essential for assessing and managing air quality, particularly in regions where O_3 pollution is a concern. The sensitivity is often quantified as the ratio of VOC to NO_x, an important parameter for characterizing the efficiency of O_3 formation in the environment. When this ratio is high, O_3 formation is constrained primarily by the availability of NO_x, leading

28

555 to what is defined as NO_x-limited or NO_x-sensitive chemistry. Consequently, taking measures to reduce NO_x emissions directly correlates with O_3 reduction. Conversely, under lower ratios, it is referred to as a VOC-limited or VOC-sensitive regime. In these scenarios, O_3 levels are notably more responsive to reductions in VOCs, and solely decreasing NO_x may not effectively lower O_3 concentrations and even worse may increase O_3 levels. Ratios between the two regimes are

560 considered transitional, and both NO_x and VOC controls may be effective.

However, it is important to acknowledge that the specific range of ratios used to define VOC and NO_x limitations can vary among researchers and depend on the specific dataset and variables under consideration. Different studies and regulatory assessments may employ distinct criteria for categorizing O_3 sensitivity to VOCs and NO_x, making it imperative to consider these variations

565 when interpreting and applying sensitivity analyses in different contexts. From an observational perspective, the HCHO concentration has been widely used as a proxy for VOC reactivity as it is a short-lived oxidation product of many VOCs and positively correlated with peroxyl radicals (Sillman, 1995), and it is also available in many observational datasets. The concentration of HCHO serves as an indicator for volatile organic compound (VOC) reactivity as it exhibits a

570 positive correlation with proxy radicals (Sillman, 1995). Sillman (1995) identified that elevated HCHO/NOy ratios typically indicate NOx-limited regimes, whereas reduced HCHO/NOy ratios are indicative of VOC-limited regimes. Satellite data, like TROPOMI (The Tropospheric Monitoring Instrument), provides daily columnar HCHO and NO_2 spatial distributions at a certain time of the day. Thus, satellite data have been widely used in determining the VOC-NO_x sensitivity

575 regimes (Duncan et al., 2010; Souri et al., 2020; Jin et al., 2017; Martin et al., 2004). In this study, we also employ the HCHO-to-NO_2 ratio (FNR) as a proxy for assessing VOC-NO_x sensitivity. Surface FNRs are usually lower by considering surface or planetary boundary layer number concentrations since the vertical distribution of HCHO and NO_2 varies as shown in Figure 12. HCHO is distributed up to 5 km, whereas NO_2 predominantly remains within 0.5 km. Various studies have

580 investigated the FNR threshold for regime determination. Schroeder et al. (2017) defined the transitional regime with FNR values ranging from 0.7 to 2.3, while Duncan et al. (2010) reported a range of 1.0 to 2.0, and Jin et al. (2020) found values of 3.2 to 4.1 using satellite column retrievals. Additionally, Acdan et al. (2022) utilized ground-based PAMS measurements and proposed an FNR range of 0.3 to 1.0 for the transition over the Lake Michigan region. In our study, we are following

585 Duncan et al. (2010) which linked FNR with surface O_3 sensitivity in model simulation and used

in several studies (Tang et al., 2012; Jin and Holloway, 2015; Souri et al., 2017) by Duncan et al. (2010). When FNR is less than 1, it is classified as VOC-limited; when it falls between 1 and 2, it is considered a transitional regime; and when FNR exceeds 2, it is defined as NO_x-limited.

In the previous section, we demonstrated a negative correlation between NO_2 and O_3 indicating that Phoenix falls within the VOC-limited/VOC-sensitive regime. To gain a more comprehensive understanding of NO_x-VOC sensitivity in the greater Phoenix metropolitan area, we calculated monthly FNR values for each year and their respective means. Figure 13 displays spatial maps of FNR across Phoenix and Tucson, highlighting grids with FNR values less than or equal to 4. The Maricopa County Non-Attainment Area (NAA) is outlined in red. Overall, central Phoenix is predominantly characterized as VOC-limited or transitional, with FNR values consistently below 2 with an average FNR of 1.15 across the metropolitan area. The FNR tends to be lower within the more densely populated urban areas. As one moves towards the suburban areas, there is an increase in FNR, marking a transition from the VOC-limited regime to the boundary between VOC-limited and NOx-limited conditions. Additionally, Phoenix exhibits lower FNR values compared to Tucson. Notably, hotspots related to fire activities are evident in different years, such as the eastern region of Phoenix in 2019, the northeastern areas of Phoenix and Tucson in 2020, and the eastern part of Phoenix in 2021. Fire and biomass burning activities typically result in significant emissions of CO, CO_2, NO_x, VOCs, particulate matter, methane, and more. Consequently, when these fire events occur, they can alter the NO_x-VOC sensitivity of the affected areas. The "pop-up" local FNR minima in Figure 13 (labeled as WF) suggests that wildfire events lead to a reduction in the FNR and a shift in the sensitivity regime towards VOC-limited. Similar results have been reported using satellite observations (Jin et al., 2017) and ground-based surface measurements (Miech et al., 2023) where they found that during the fire event, the NO_x values are high near the fire leading to lower FNRs. The varying contours from year to year indicate slight differences in sensitivities between those years, with 2019 and 2020 showing lower mean FNR values over the NAA compared to other years.
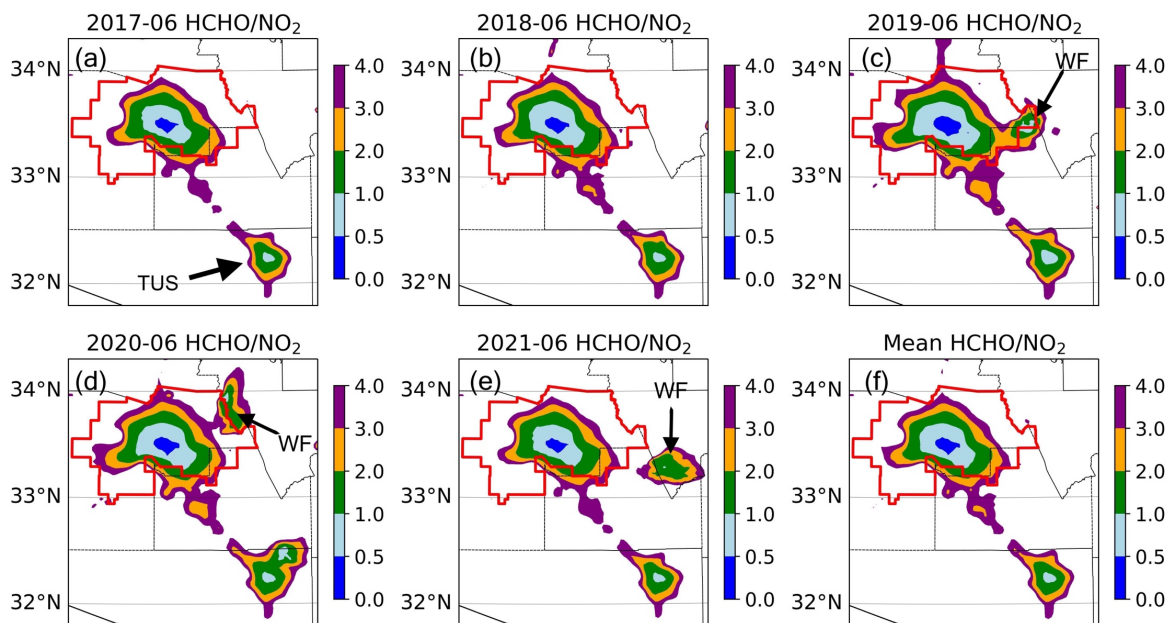
Figure 13. WRF-Chem simulated monthly mean ratio of surface HCHO/NO₂ over Phoenix and Tucson. Red lines represent the nonattainment area designated by the EPA. "WF" denotes instances of "pop-up" low FNRs resulting from wildfire events.

In Figure 14, we present scatter plots illustrating the relationship between hourly surface concentrations of NO_2 and HCHO in three cities: Phoenix, Tucson, and Yuma, as simulated by WRF-Chem. The color gradients in these scatter plots correspond to the respective O_3 concentrations (panels a-c) and FNR values (panels d-f).

When we compare Figure 14(a) with 14(d), we observe that in Phoenix, elevated O_3 concentrations are linked to lower NO_2 levels (as also seen in Figure 11) and high HCHO concentrations, falling within the range of 0.5 to 1.2 in terms of FNR. Conversely, the lowest O_3 levels occur when NO_2 levels are relatively high. In Tucson, NO_2 levels are approximately half of those observed in Phoenix, and O_3 occurrences are less frequent. Higher O_3 concentrations in Tucson are primarily associated with FNR values greater than 1. Yuma, on the other hand, exhibits the lowest levels of NO_2, but it has the highest HCHO concentrations, also accompanied by high O_3 levels. Notably, the mean FNR in Yuma is also the highest among the three cities, as indicated by the prominent red color in Figure 14(f).

Understanding these correlations between HCHO, NO_2, and O_3 levels is crucial for formulating effective regulatory strategies aimed at mitigating O_3 pollution in urban settings resulting from

localized O₃ production. The transitional regime observed in the Phoenix metropolitan area suggests that while additional reductions in NO₂ levels could potentially decrease O₃ design values, there exists the possibility of concurrent increases in daily mean O₃ levels due to the intricate interplay of diurnal complex O₃ production. In Yuma, where higher HCHO levels prevail, reducing VOC emissions may serve as a viable approach to lowering O₃ concentrations.
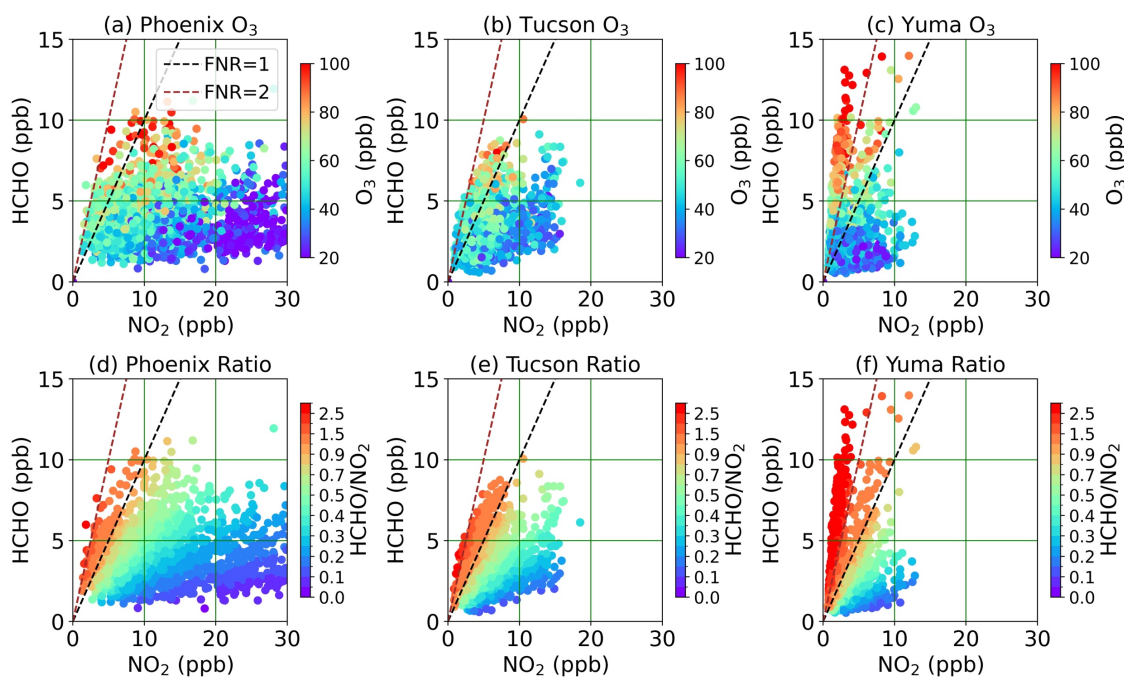

Figure 14. Scatter plots of WRF-Chem simulated hourly surface NO₂ versus HCHO concentrations at three cities: Phoenix, Tucson, Yuma. The colors represent the corresponding O₃ concentrations (top) and ratio of HCHO/NO₂ (FNR; bottom) for years from 2017 to 2021. Black and brown dash lines represent the FNR values of 1 and 2, respectively.

4. Conclusion

In this study, our primary objective was to gain a comprehensive understanding of surface O₃ pollution in an arid/semi-arid climate region, with a specific focus on the state of Arizona as a representative case study. To achieve this, we employed WRF-Chem simulations to simulate O₃ and various other gases, examining the month of June within a five-year period spanning from 2017 to 2021. Our model's performance was assessed by comparison with surface observations from the EPA AQS and PAMS monitoring networks, as well as a CMAQ reanalysis product. Our analysis primarily focused on three major cities within Arizona: Phoenix, Tucson, and Yuma. We

calculated statistics for both hourly and MDA8 O_3 concentrations. We also examined additional monthly mean fields, including key meteorological parameters (T, RH, wind), and air pollutants (NO_2, CO, VOCs). Results show that WRF-Chem demonstrated better performance in simulating MDA8 O_3 compared to hourly O_3. The model exhibited a tendency to overestimate nighttime NO_2 levels, resulting in larger biases during the night; the model also shows an overestimate of surface NO_2 in Phoenix and an underestimate of NO_2 in Tucson. Among the cities examined, Yuma displayed the highest mean error and a positive bias, whereas Phoenix and Tucson showed closer agreement with observations, featuring smaller errors and negative biases. Furthermore, our evaluation indicated minimal biases in the representation of meteorological parameters. However, for VOCs, the model underestimated their surface concentrations.

O_3 exceedances were also investigated and evaluated at all available AQS monitoring sites in Maricopa County. Our model exhibited strong agreement with site measurements regarding both the magnitude and the number of days on which an O_3 exceedance occurred considering factors such as location, number of days, spatial extent, and spatial variability. The analysis of an O_3 exceedance case beginning on 13 June 2017, along with the back trajectories, suggests that Arizona can also be affected by long-range transport from interstate or continental sources.

To better understand the O_3 formation in this arid/semi-arid region, we examined the correlation between O_3 and other factors influencing O_3 production. In Phoenix, the scatter plots exhibited overall negative correlations between O_3 and CO, NO_2, and RH, while positive correlations were strongly observed with T and HCHO. These correlations suggest that O_3 levels are higher when NO_2 concentrations are generally lower and HCHO concentrations are higher, indicating that the central Phoenix falls within the VOC-limited regime. Additionally, our spatial maps of the FNR confirm that in the most densely populated urban areas, the region predominantly falls within the VOC-limited regime, with FNR less than 1. Moving outward the area FNR values increase, indicating a shift to a transitional and NOx-limited regime. This analysis significantly contributes to our understanding of O_3 dynamics in arid and semi-arid regions and has implications for air quality management and policy in such environments.

In terms of the uncertainties associated with the approached in this study, they are largely dependent on the bias and uncertainty inherent in the emissions data used for our model simulations. In the case of anthropogenic emissions, our utilization of NEI2017 data for years other

than the reference year introduces potential errors due to variations in emissions over time. This particularly affects the representation of precursor pollutants, notably NO_x. Moreover, the underestimation of HCHO and other biogenic emissions simulated from MEGAN 2.1 may also

675 contribute to a negative bias in the FNR, leading to the bias in regime determination. Additionally, Dust events are particularly common in Arizona, especially in the southwest region where the Sonora Desert is situated. The presence of dust can significantly impact ozone photolysis dynamics by interacting with sunlight. Dust particles can scatter and absorb solar radiation, thereby altering the photolysis rates of ozone molecules in the atmosphere. Consequently, these events may

680 introduce bias to our findings. However, according to Lader et al. (2016) and Ardon-Dryer et al. (2023), dust storm events are most frequent during the Monsoon season (in July and August), typically peaking around 6-7 pm when photolysis rates are at their lowest. Focusing on the dry summer month of June in this study helps alleviate the bias caused by these dust events.

However, a better performance of the model can be pursued through various strategies. While

685 achieving a higher spatial resolution, such as 1 km, is desirable, it remains constrained by the available computational resources and the resolution of input datasets, for instance, the NEI currently operating at 4 km resolution. A potential remedy involves employing a finer-resolution emission dataset, such as the Neighborhood Emission Mapping Operation (NEMO) proposed by Ma and Tong (2022). Additionally, refining simulations of nighttime chemistry, crucial for

690 accurate predictions, necessitates a more precise estimation of the PBLH, which, if improved, can contribute to reducing the O_3 bias during nocturnal hours. This improvement can be achieved by assimilating PBLH estimates obtained from radiosonde and ceilometer data.

For future work, we aim to continue investigating the contributions of individual sources of O_3 to total O_3 levels. We will adopt a tagging technique developed by Emmons et al. (2012) and Butler

695 et al. (2018). This tagging technique uses the WRF-Chem model with the MOZART gas chemistry mechanism to attribute the sources contributing to tropospheric O_3. We will focus on the contributions from anthropogenic, fire, and biogenic emissions, and also use the model to trace the transport of O_3 and its precursors (NO_x, VOC) from their source.

700

Code and Data Availability Statement.

The WRF-Chem model is version 4.4 is available for download from ZENODO (doi: 10.5281/zenodo.10479471) and publicly available at NCAR https://www2.mmm.ucar.edu/wrf/users/download/get_source.html (last access: 25 June 2022). The model outputs, ADEQ forecast, and CMAQ reanalysis datasets can be provided upon request to the corresponding author. EPA AQS and PAMS hourly and daily datasets are available at https://aqs.epa.gov/aqsweb/airdata/download_files.html.

Author contributions.

YG and AA designed the research. YG performed the model runs and subsequent analysis. YG wrote the paper with contributions from AA and AS. RK provided the reanalysis dataset, AM and CR helped with the observational data acquisition and preprocessing.

References:

730 Acdan, J. J. M., Pierce, R. B., Dickens, A. F., Adelman, Z., and Nergui, T.: Ozone–NOx–VOC Sensitivity of the Lake Michigan Region Inferred from TROPOMI Observations and Ground-Based Measurements, EGUsphere, 2022, 1-38, 10.5194/egusphere-2022-1154, 2022.

Achakulwisut, P., Anenberg, S. C., Neumann, J. E., Penn, S. L., Weiss, N., Crimmins, A., Fann, N., Martinich, J., Roman, H., and Mickley, L. J.: Effects of Increasing Aridity on Ambient Dust
735 and Public Health in the U.S. Southwest Under Climate Change, GeoHealth, 3, 127-144, https://doi.org/10.1029/2019GH000187, 2019.

Anderson, H. R.: Air pollution and mortality: A history, Atmospheric Environment, 43, 142-152, https://doi.org/10.1016/j.atmosenv.2008.09.026, 2009.

Ardon-Dryer, K., Gill, T. E., and Tong, D. Q.: When a Dust Storm Is Not a Dust Storm:
740 Reliability of Dust Records From the Storm Events Database and Implications for Geohealth Applications, Geohealth, 7, e2022GH000699, 10.1029/2022gh000699, 2023.

Asadi Zarch, M. A., Sivakumar, B., Malekinezhad, H., and Sharma, A.: Future aridity under conditions of global climate change, Journal of Hydrology, 554, 451-469, https://doi.org/10.1016/j.jhydrol.2017.08.043, 2017.

745 Betito, G., Arellano, A., and Sorooshian, A.: Influence of Transboundary Pollution on the Variability of Surface Ozone Concentrations in the Desert Southwest of the U.S.: Case Study for Arizona, Atmosphere, 15, 401, 10.3390/atmos15040401, 2024.

Betito, G., Sorooshian, A., and Arellano, A.: Influence of transboundary pollution on the variability of surface ozone concentration in the Desert Southwest of the U.S.: Case study for
750 Arizona, ACS ES&T Air, under review, 2023.

Butler, T., Lupascu, A., and Nalam, A.: Attribution of ground-level ozone to anthropogenic and natural sources of nitrogen oxides and reactive carbon in a global chemical transport model, Atmos. Chem. Phys., 20, 10707-10731, 10.5194/acp-20-10707-2020, 2020.

Butler, T., Lupascu, A., Coates, J., and Zhu, S.: TOAST 1.0: Tropospheric Ozone Attribution of
755 Sources with Tagging for CESM 1.2.2, Geosci. Model Dev., 11, 2825-2840, 10.5194/gmd-11-2825-2018, 2018.

Carrillo-Torres, E. R., Hernández-Paniagua, I. Y., and Mendoza, A.: Use of Combined Observational- and Model-Derived Photochemical Indicators to Assess the O3-NOx-VOC System Sensitivity in Urban Areas, Atmosphere, 8, 22, 2017.

760 Cheng, Y., Huang, X.-F., Peng, Y., Tang, M.-X., Zhu, B., Xia, S.-Y., and He, L.-Y.: A novel machine learning method for evaluating the impact of emission sources on ozone formation, Environmental Pollution, 316, 120685, https://doi.org/10.1016/j.envpol.2022.120685, 2023.

Chin, M., Ginoux, P., Kinne, S., Torres, O., Holben, B. N., Duncan, B. N., Martin, R. V., Logan, J. A., Higurashi, A., and Nakajima, T.: Tropospheric Aerosol Optical Thickness from the
765 GOCART Model and Comparisons with Satellite and Sun Photometer Measurements, Journal of the Atmospheric Sciences, 59, 461-483, https://doi.org/10.1175/1520-0469(2002)059<0461:TAOTFT>2.0.CO;2, 2002.

Cooper, O. R., Gao, R.-S., Tarasick, D., Leblanc, T., and Sweeney, C.: Long-term ozone trends at rural ozone monitoring sites across the United States, 1990–2010, Journal of Geophysical Research: Atmospheres, 117, https://doi.org/10.1029/2012JD018261, 2012.

Demerjian, K. L.: A review of national monitoring networks in North America, Atmospheric Environment, 34, 1861-1884, https://doi.org/10.1016/S1352-2310(99)00452-5, 2000.

Dimitriou, K. and Kassomenos, P.: Three year study of tropospheric ozone with back trajectories at a metropolitan and a medium scale urban area in Greece, Science of The Total Environment, 502, 493-501, https://doi.org/10.1016/j.scitotenv.2014.09.072, 2015.

Duan, J., Tan, J., Yang, L., Wu, S., and Hao, J.: Concentration, sources and ozone formation potential of volatile organic compounds (VOCs) during ozone episode in Beijing, Atmospheric Research, 88, 25-35, https://doi.org/10.1016/j.atmosres.2007.09.004, 2008.

Duncan, B. N., Yoshida, Y., Olson, J. R., Sillman, S., Martin, R. V., Lamsal, L., Hu, Y., Pickering, K. E., Retscher, C., Allen, D. J., and Crawford, J. H.: Application of OMI observations to a space-based indicator of NOx and VOC controls on surface ozone formation, Atmospheric Environment, 44, 2213-2223, https://doi.org/10.1016/j.atmosenv.2010.03.010, 2010.

Emmons, L. K., Hess, P. G., Lamarque, J. F., and Pfister, G. G.: Tagged ozone mechanism for MOZART-4, CAM-chem and other chemical transport models, Geosci. Model Dev., 5, 1531-1542, 10.5194/gmd-5-1531-2012, 2012.

Emmons, L. K., Walters, S., Hess, P. G., Lamarque, J. F., Pfister, G. G., Fillmore, D., Granier, C., Guenther, A., Kinnison, D., Laepple, T., Orlando, J., Tie, X., Tyndall, G., Wiedinmyer, C., Baughcum, S. L., and Kloster, S.: Description and evaluation of the Model for Ozone and Related chemical Tracers, version 4 (MOZART-4), Geosci. Model Dev., 3, 43-67, 10.5194/gmd-3-43-2010, 2010.

EPA: Nitrogen Dioxide Trends, https://www.epa.gov/air-trends/nitrogen-dioxide-trends, 2023.

Fang, T., Zhu, Y., Wang, S., Xing, J., Zhao, B., Fan, S., Li, M., Yang, W., Chen, Y., and Huang, R.: Source impact and contribution analysis of ambient ozone using multi-modeling approaches over the Pearl River Delta region, China, Environmental Pollution, 289, 117860, https://doi.org/10.1016/j.envpol.2021.117860, 2021.

Fiore, A. M., Jacob, D. J., Bey, I., Yantosca, R. M., Field, B. D., Fusco, A. C., and Wilkinson, J. G.: Background ozone over the United States in summer: Origin, trend, and contribution to pollution episodes, Journal of Geophysical Research: Atmospheres, 107, ACH 11-11-ACH 11-25, https://doi.org/10.1029/2001JD000982, 2002.

Freitas, S. R., Longo, K. M., Chatfield, R., Latham, D., Silva Dias, M. A. F., Andreae, M. O., Prins, E., Santos, J. C., Gielow, R., and Carvalho Jr, J. A.: Including the sub-grid scale plume rise of vegetation fires in low resolution atmospheric transport models, Atmos. Chem. Phys., 7, 3385-3398, 10.5194/acp-7-3385-2007, 2007.

Geron, C., Guenther, A., Greenberg, J., Karl, T., and Rasmussen, R.: Biogenic volatile organic compound emissions from desert vegetation of the southwestern US, Atmospheric Environment, 40, 1645-1660, 10.1016/j.atmosenv.2005.11.011, 2006.

Grell, G. A. and Freitas, S. R.: A scale and aerosol aware stochastic convective parameterization for weather and air quality modeling, Atmos. Chem. Phys., 14, 5233-5250, 10.5194/acp-14-5233-2014, 2014.

Guenther, A.: Estimates of global terrestrial isoprene emissions using MEGAN (Model of Emissions of Gases and Aerosols from Nature), Atmospheric Chemistry and Physics, 7, 4327-4327, 10.5194/acp-6-3181-2006, 2007.

Guenther, A., Karl, T., Harley, P., Wiedinmyer, C., Palmer, P. I., and Geron, C.: Estimates of global terrestrial isoprene emissions using MEGAN (Model of Emissions of Gases and Aerosols from Nature), Atmos. Chem. Phys., 6, 3181-3210, 10.5194/acp-6-3181-2006, 2006.

Guenther, A. B., Jiang, X., Heald, C. L., Sakulyanontvittaya, T., Duhl, T., Emmons, L. K., and Wang, X.: The Model of Emissions of Gases and Aerosols from Nature version 2.1 (MEGAN2.1): an extended and updated framework for modeling biogenic emissions, Geosci. Model Dev., 5, 1471-1492, 10.5194/gmd-5-1471-2012, 2012.

He, Z., Wang, X., Ling, Z., Zhao, J., Guo, H., Shao, M., and Wang, Z.: Contributions of different anthropogenic volatile organic compound sources to ozone formation at a receptor site in the Pearl River Delta region and its policy implications, Atmos. Chem. Phys., 19, 8801-8816, 10.5194/acp-19-8801-2019, 2019.

Hong, S.-Y.: A new stable boundary-layer mixing scheme and its impact on the simulated East Asian summer monsoon, Quarterly Journal of the Royal Meteorological Society, 136, 1481-1496, https://doi.org/10.1002/qj.665, 2010.

Huang, J., Li, Y., Fu, C., Chen, F., Fu, Q., Dai, A., Shinoda, M., Ma, Z., Guo, W., Li, Z., Zhang, L., Liu, Y., Yu, H., He, Y., Xie, Y., Guan, X., Ji, M., Lin, L., Wang, S., Yan, H., and Wang, G.: Dryland climate change: Recent progress and challenges, Reviews of Geophysics, 55, 719-778, https://doi.org/10.1002/2016RG000550, 2017.

Iacono, M. J., Delamere, J. S., Mlawer, E. J., Shephard, M. W., Clough, S. A., and Collins, W. D.: Radiative forcing by long-lived greenhouse gases: Calculations with the AER radiative transfer models, Journal of Geophysical Research: Atmospheres, 113, https://doi.org/10.1029/2008JD009944, 2008.

Iriti, M. and Faoro, F.: Chemical Diversity and Defence Metabolism: How Plants Cope with Pathogens and Ozone Pollution, International Journal of Molecular Sciences, 10, 3371-3399, 2009.

Jacob, D. J.: Heterogeneous chemistry and tropospheric ozone, Atmospheric Environment, 34, 2131-2159, https://doi.org/10.1016/S1352-2310(99)00462-8, 2000.

Jin, X. and Holloway, T.: Spatial and temporal variability of ozone sensitivity over China observed from the Ozone Monitoring Instrument, Journal of Geophysical Research: Atmospheres, 120, 7229-7246, https://doi.org/10.1002/2015JD023250, 2015.

Jin, X., Fiore, A., Boersma, K. F., Smedt, I. D., and Valin, L.: Inferring Changes in Summertime Surface Ozone–NOx–VOC Chemistry over U.S. Urban Areas from Two Decades of Satellite and Ground-Based Observations, Environmental Science & Technology, 54, 6518-6529, 10.1021/acs.est.9b07785, 2020.

Jin, X., Fiore, A. M., Murray, L. T., Valin, L. C., Lamsal, L. N., Duncan, B., Boersma, K. F., De Smedt, I., Abad, G. G., Chance, K., and Tonnesen, G. S.: Evaluating a Space-Based Indicator of Surface Ozone-NO (x) -VOC Sensitivity Over Midlatitude Source Regions and Application to Decadal Trends, J Geophys Res Atmos, 122, 10-461, 10.1002/2017jd026720, 2017.

Kalogridis, C., Gros, V., Sarda-Esteve, R., Langford, B., Loubet, B., Bonsang, B., Bonnaire, N., Nemitz, E., Genard, A. C., Boissard, C., Fernandez, C., Ormeño, E., Baisnée, D., Reiter, I., and Lathière, J.: Concentrations and fluxes of isoprene and oxygenated VOCs at a French Mediterranean oak forest, Atmos. Chem. Phys., 14, 10085-10102, 10.5194/acp-14-10085-2014, 2014.

Lader, G., Raman, A. , Davis, J. , & Waters, K.: Blowing Dust and Dust Storms: One of Arizona's Most Underrated Weathe Hazards 2016.

Lamarque, J. F., Emmons, L. K., Hess, P. G., Kinnison, D. E., Tilmes, S., Vitt, F., Heald, C. L., Holland, E. A., Lauritzen, P. H., Neu, J., Orlando, J. J., Rasch, P. J., and Tyndall, G. K.: CAM-chem: description and evaluation of interactive atmospheric chemistry in the Community Earth System Model, Geosci. Model Dev., 5, 369-411, 10.5194/gmd-5-369-2012, 2012.

Li, J., Georgescu, M., Hyde, P., Mahalov, A., and Moustaoui, M.: Regional-scale transport of air pollutants: impacts of Southern California emissions on Phoenix ground-level ozone concentrations, Atmos. Chem. Phys., 15, 9345-9360, 10.5194/acp-15-9345-2015, 2015.

Lippmann, M.: HEALTH EFFECTS OF OZONE A Critical Review, JAPCA, 39, 672-695, 10.1080/08940630.1989.10466554, 1989.

Liu, C. and Shi, K.: A review on methodology in O3-NOx-VOC sensitivity study, Environmental Pollution, 291, 118249, https://doi.org/10.1016/j.envpol.2021.118249, 2021.

Lupașcu, A. and Butler, T.: Source attribution of European surface O3 using a tagged O3 mechanism, Atmos. Chem. Phys., 19, 14535-14558, 10.5194/acp-19-14535-2019, 2019.

Ma, S. and Tong, D. Q.: Neighborhood Emission Mapping Operation (NEMO): A 1-km anthropogenic emission dataset in the United States, Scientific Data, 9, 680, 10.1038/s41597-022-01790-9, 2022.

Manisalidis, I., Stavropoulou, E., Stavropoulos, A., and Bezirtzoglou, E.: Environmental and Health Impacts of Air Pollution: A Review, Frontiers in Public Health, 8, 10.3389/fpubh.2020.00014, 2020.

Martin, R. V., Fiore, A. M., and Van Donkelaar, A.: Space-based diagnosis of surface ozone sensitivity to anthropogenic emissions, Geophysical Research Letters, 31, https://doi.org/10.1029/2004GL019416, 2004.

Miech, J. A., Herckes, P., Fraser, M., Arellano, A., Mirrezaei, M. A., and Guo, Y.: NO2 & O3 Photochemistry Impacted by Wildfire Smoke, Atmospheric Environment, under review, 2023.

Mishra, M., Chen, P.-H., Bisquera, W., Lin, G.-Y., Le, T.-C., Dejchanchaiwong, R., Tekasakul, P., Jhang, C.-W., Wu, C.-J., and Tsai, C.-J.: Source-apportionment and spatial distribution analysis of VOCs and their role in ozone formation using machine learning in central-west Taiwan, Environmental Research, 232, 116329, https://doi.org/10.1016/j.envres.2023.116329, 2023.

Monin, A. S. and Obukhov, A. M.: Basic Laws of Turbulent Mixing in the Surface Layer of the Atmosphere, SSSR, 163-187,

890   Monks, P. S., Archibald, A. T., Colette, A., Cooper, O., Coyle, M., Derwent, R., Fowler, D., Granier, C., Law, K. S., Mills, G. E., Stevenson, D. S., Tarasova, O., Thouret, V., von Schneidemesser, E., Sommariva, R., Wild, O., and Williams, M. L.: Tropospheric ozone and its precursors from the urban to the global scale from air quality to short-lived climate forcer, Atmos. Chem. Phys., 15, 8889-8973, 10.5194/acp-15-8889-2015, 2015.

895   Morrison, E. C., Drewer, J., and Heal, M. R.: A comparison of isoprene and monoterpene emission rates from the perennial bioenergy crops short-rotation coppice willow and Miscanthus and the annual arable crops wheat and oilseed rape, GCB Bioenergy, 8, 211-225, https://doi.org/10.1111/gcbb.12257, 2016.

Morrison, H., Thompson, G., and Tatarskii, V.: Impact of Cloud Microphysics on the
900   Development of Trailing Stratiform Precipitation in a Simulated Squall Line: Comparison of One- and Two-Moment Schemes, Monthly Weather Review, 137, 991-1007, https://doi.org/10.1175/2008MWR2556.1, 2009.

NWS Phoenix: Year in Review 2020, https://www.weather.gov/psr/YearinReview2020v2, 2020.

Odman, M. T., Hu, Y., Russell, A. G., Hanedar, A., Boylan, J. W., and Brewer, P. F.:
905   Quantifying the sources of ozone, fine particulate matter, and regional haze in the Southeastern United States, Journal of Environmental Management, 90, 3155-3168, https://doi.org/10.1016/j.jenvman.2009.05.028, 2009.

Oleson, K., Lawrence, D., B, G., Flanner, M., Kluzek, E., Lawrence, P., Levis, S., Swenson, S., Thornton, E., Feddema, J., Heald, C., Lamarque, J.-F., Niu, G.-Y., Qian, T., Running, S.,
910   Sakaguchi, K., Yang, Z.-L., Zeng, X., and Zeng, X.: Technical Description of version 4.0 of the Community Land Model (CLM), 2010.

Parrish, D. D., Faloona, I. C., and Derwent, R. G.: Observational-based assessment of contributions to maximum ozone concentrations in the western United States, Journal of the Air & Waste Management Association, 72, 434-454, 10.1080/10962247.2022.2050962, 2022.

915   Paul, R. S., Andrew, C. C., Gregory, D. P., Kurt, A., and Malcolm, K. H.: The climate of the US Southwest, Climate Research, 21, 219-238, 2002.

Qu, Z., Wu, D., Henze, D. K., Li, Y., Sonenberg, M., and Mao, F.: Transboundary transport of ozone pollution to a US border region: A case study of Yuma, Environmental Pollution, 273, 116421, https://doi.org/10.1016/j.envpol.2020.116421, 2021.

920   Reich, P. B.: Quantifying plant response to ozone: a unifying theory, Tree Physiology, 3, 63-91, 10.1093/treephys/3.1.63, 1987.

Rolph, G., Stein, A., and Stunder, B.: Real-time Environmental Applications and Display sYstem: READY, Environmental Modelling & Software, 95, 210-228, https://doi.org/10.1016/j.envsoft.2017.06.025, 2017.

925   Schroeder, J. R., Crawford, J. H., Fried, A., Walega, J., Weinheimer, A., Wisthaler, A., Müller, M., Mikoviny, T., Chen, G., Shook, M., Blake, D. R., and Tonnesen, G. S.: New insights into the column CH2O/NO2 ratio as an indicator of near-surface ozone sensitivity, Journal of

Geophysical Research: Atmospheres, 122, 8885-8907, https://doi.org/10.1002/2017JD026781, 2017.

930   Sillman, S.: The use of NOy, H2O2 and HNO3 as indicators for ozone-NOx-hydrocarbon sensitivity in urban locations, Journal of Geophysical Research: Atmospheres, 100, 14175-14188, 10.1029/94JD02953, 1995.

Sillman, S. and He, D.: Some theoretical results concerning O3-NOx-VOC chemistry and NOx-VOC indicators, Journal of Geophysical Research: Atmospheres, 107, ACH 26-21-ACH 26-15,
935   https://doi.org/10.1029/2001JD001123, 2002.

Sillman, S., Vautard, R., Menut, L., and Kley, D.: O3-NOx-VOC sensitivity and NOx-VOC indicators in Paris: Results from models and Atmospheric Pollution Over the Paris Area (ESQUIF) measurements, Journal of Geophysical Research: Atmospheres, 108, https://doi.org/10.1029/2002JD001561, 2003.

940   Sorooshian, A., Arellano, A. F., Fraser, M. P., Herckes, P., Betito, G., Betterton, E. A., Braun, R. A., Guo, Y., Mirrezaei, M. A., and Roychoudhury, C.: Ozone in the Desert Southwest of the United States: A Synthesis of Past Work and Steps Ahead, ACS ES&T Air, 1, 62-79, 10.1021/acsestair.3c00033, 2024.

Souri, A. H., Choi, Y., Jeon, W., Woo, J.-H., Zhang, Q., and Kurokawa, J.-i.: Remote sensing
945   evidence of decadal changes in major tropospheric ozone precursors over East Asia, Journal of Geophysical Research: Atmospheres, 122, 2474-2492, https://doi.org/10.1002/2016JD025663, 2017.

Souri, A. H., Nowlan, C. R., Wolfe, G. M., Lamsal, L. N., Chan Miller, C. E., Abad, G. G., Janz, S. J., Fried, A., Blake, D. R., Weinheimer, A. J., Diskin, G. S., Liu, X., and Chance, K.:
950   Revisiting the effectiveness of HCHO/NO2 ratios for inferring ozone sensitivity to its precursors using high resolution airborne remote sensing observations in a high ozone episode during the KORUS-AQ campaign, Atmospheric Environment, 224, 117341, https://doi.org/10.1016/j.atmosenv.2020.117341, 2020.

Stein, A. F., Draxler, R. R., Rolph, G. D., Stunder, B. J. B., Cohen, M. D., and Ngan, F.:
955   NOAA's HYSPLIT Atmospheric Transport and Dispersion Modeling System, Bulletin of the American Meteorological Society, 96, 2059-2077, https://doi.org/10.1175/BAMS-D-14-00110.1, 2015.

Straffelini, E. and Tarolli, P.: Climate change-induced aridity is affecting agriculture in Northeast Italy, Agricultural Systems, 208, 103647, https://doi.org/10.1016/j.agsy.2023.103647, 2023.

960   Sudo, K. and Akimoto, H.: Global source attribution of tropospheric ozone: Long-range transport from various source regions, Journal of Geophysical Research: Atmospheres, 112, https://doi.org/10.1029/2006JD007992, 2007.

Tang, G., Wang, Y., Li, X., Ji, D., Hsu, S., and Gao, X.: Spatial-temporal variations in surface ozone in Northern China as observed during 2009–2010 and possible implications for future air
965   quality control strategies, Atmos. Chem. Phys., 12, 2757-2776, 10.5194/acp-12-2757-2012, 2012.

Tewari, M., Wang, W., Dudhia, J., LeMone, M. A., Mitchell, K., Ek, M., Gayno, G., Wegiel, J., and Cuenca, R.: Implementation and verification of the united NOAH land surface model in the

WRF model, 20th Conference on Weather Analysis and Forecasting/16th Conference on Numerical Weather Prediction2004.

Tilmes, S., Lamarque, J. F., Emmons, L. K., Kinnison, D. E., Ma, P. L., Liu, X., Ghan, S., Bardeen, C., Arnold, S., Deeter, M., Vitt, F., Ryerson, T., Elkins, J. W., Moore, F., Spackman, J. R., and Val Martin, M.: Description and evaluation of tropospheric chemistry and aerosols in the Community Earth System Model (CESM1.2), Geosci. Model Dev., 8, 1395-1426, 10.5194/gmd-8-1395-2015, 2015.

Trainer, M., Parrish, D. D., Goldan, P. D., Roberts, J., and Fehsenfeld, F. C.: Review of observation-based analysis of the regional factors influencing ozone concentrations, Atmospheric Environment, 34, 2045-2061, https://doi.org/10.1016/S1352-2310(99)00459-8, 2000.

Vingarzan, R.: A review of surface ozone background levels and trends, Atmospheric Environment, 38, 3431-3442, https://doi.org/10.1016/j.atmosenv.2004.03.030, 2004.

Wang, T., Xue, L., Brimblecombe, P., Lam, Y. F., Li, L., and Zhang, L.: Ozone pollution in China: A review of concentrations, meteorological influences, chemical precursors, and effects, Science of The Total Environment, 575, 1582-1596, https://doi.org/10.1016/j.scitotenv.2016.10.081, 2017.

Weng, X., Forster, G. L., and Nowack, P.: A machine learning approach to quantify meteorological drivers of ozone pollution in China from 2015 to 2019, Atmos. Chem. Phys., 22, 8385-8402, 10.5194/acp-22-8385-2022, 2022.

Wiedinmyer, C., Kimura, Y., McDonald-Buller, E. C., Emmons, L. K., Buchholz, R. R., Tang, W., Seto, K., Joseph, M. B., Barsanti, K. C., Carlton, A. G., and Yokelson, R.: The Fire Inventory from NCAR version 2.5: an updated global fire emissions model for climate and chemistry applications, Geosci. Model Dev., 16, 3873-3891, 10.5194/gmd-16-3873-2023, 2023.

Xiong, Y. and Du, K.: Source-resolved attribution of ground-level ozone formation potential from VOC emissions in Metropolitan Vancouver, BC, Science of The Total Environment, 721, 137698, https://doi.org/10.1016/j.scitotenv.2020.137698, 2020.

Yang, L., Xie, D., Yuan, Z., Huang, Z., Wu, H., Han, J., Liu, L., and Jia, W.: Quantification of Regional Ozone Pollution Characteristics and Its Temporal Evolution: Insights from Identification of the Impacts of Meteorological Conditions and Emissions, Atmosphere, 12, 279, 2021.

Zare, A., Christensen, J. H., Gross, A., Irannejad, P., Glasius, M., and Brandt, J.: Quantifying the contributions of natural emissions to ozone and total fine PM concentrations in the Northern Hemisphere, Atmos. Chem. Phys., 14, 2735-2756, 10.5194/acp-14-2735-2014, 2014.

Zaveri, R. A., Berkowitz, C. M., Kleinman, L. I., Springston, S. R., Doskey, P. V., Lonneman, W. A., and Spicer, C. W.: Ozone production efficiency and NOx depletion in an urban plume: Interpretation of field observations and implications for evaluating O3-NOx-VOC sensitivity, Journal of Geophysical Research: Atmospheres, 108, https://doi.org/10.1029/2002JD003144, 2003.

Zhan, J., Ma, W., Song, B., Wang, Z., Bao, X., Xie, H. B., Chu, B., He, H., Jiang, T., and Liu, Y.: The contribution of industrial emissions to ozone pollution: identified using ozone formation path tracing approach, NPJ Clim Atmos Sci, 6, 37, 10.1038/s41612-023-00366-7, 2023.

1010   Zhang, Y., Wang, X., Blake, D. R., Li, L., Zhang, Z., Wang, S., Guo, H., Lee, F. S. C., Gao, B., Chan, L., Wu, D., and Rowland, F. S.: Aromatic hydrocarbons as ozone precursors before and after outbreak of the 2008 financial crisis in the Pearl River Delta region, south China, Journal of Geophysical Research: Atmospheres, 117, https://doi.org/10.1029/2011JD017356, 2012.